

Muhammad Fuad Nur Rochim, Indri Yaningsih, Heru Sukanto

The Effect Of Cutting Fluids And Cutting Speeds To The Vibrations Of Milling Cnc Machine

Alfan Adha Hutama Putra, Agung Tri Wijayanta, Indri Yaningsi

Experimental Studies Of Twist Ratio Effect To The Heat Transfer Enhancement Using Square Cut Tape And Classical Tape Insert

Indra Setyawan, Agung Tri Wijayanta, Tri Istanto

Experimental Study The Effect Of Slant Angle On The Improvement Of Heat Transfer In Copper Pipe Concentric Exporter With Louvered Strip Insert Forward Structure

Latif Ngudi Wibawanto, Budi Santoso, Wibawa Endra Juwana

Two-Phase Flow Characteristics On The Extensive Expansion Channel

Heri Suprianto, Eko Prasetyo Budiana, Purwadi Joko Widodo

Natural Convection Numeric Simulation On Metal Freezing Using Differential Method

M. Taufik Burhany Hendrowarsito, Wijang Wisnu Raharjo, Dwi Aries Himawanto

Fiber Weight Fraction Effect To Acoustic Properties Of Rhdpe Cantula Composite

ISSN: 1412 - 7962

mekanika

Mechanical Engineering Scientific Magazine

EDITORIAL BOARD

Editor in Chief

Ubaidillah, ST, M.Sc., Ph.D

Associate Editor

Prof. Dr. Kuncoro Dihardjo, ST, MT Prof. Dr. Muhammad Nizam, ST, MT Prof. Dr. Dwi Aries Himawanto, ST, MT Prof. Dr. techn. Suvitno, ST, MT Dr. Eng. Syamsul Hadi, ST, MT Agung Tri Wijayanta, ST, M.Sc, Ph.D Dr. Budi Santoso, ST,MT Dr. Budi Kristiawan, ST, MT D. Danardono, DPT, ST, MT, Ph.D Dr. Triyono, ST, MT Dr. Joko Triyono, ST, MT Dr. Eko Surojo, ST, MT Dr. Nurul Muhayat, ST, MT Dr. Zainal Arifin, ST, MT Prof. Ir. Dr. Saiful Amri Mazlan Fitrian Imaduddin, ST, M.Sc, Ph.D

Editorial Assistance

Ariyo Nurachman Satiya Permata, ST

Editorial Address

Mechanical Engineering Department Faculty of Engineering
Universitas Sebelas Maret

Jalan Ir. Sutami 36A Surakarta 57126

Telp. (0271) 632163

Fax. (0271) 662118

Website http://jurnal.ft.uns.ac.id/index.php/mekanika E-mail: mekanika_jtmuns@yahoo.com

Editors invite Academician, Researcher, Practitioner, and Professional to contribute an article in mechanical engineering field which is a research or literature review that have not been published on other media. It is issued twice time in a year which are in March and September. The manuscript has been accepted by editorial not more than two months before the publication. It is preferred to post it via e-mail.

mekanika

Mechanical Engineering Scientific Magazine

ISSN 1412 – 7962, Volume 16 Number 2, September 2017				
The Effect Of Cutting Fluids And Cutting Speeds To The Vibrations Of Milling Cnc Machine Muhammad Fuad Nur Rochim, Indri Yaningsih, Heru Sukanto	1-9			
Experimental Studies Of Twist Ratio Effect To The Heat Transfer Enhancement Using Square Cut Tape And Classical Tape Insert Alfan Adha Hutama Putra, Agung Tri Wijayanta, Indri Yaningsih	10-17			
Experimental Study The Effect Of Slant Angle On The Improvement Of Heat Transfer In Copper Pipe Concentric Exporter With Louvered Strip Insert Forward Structure Indra Setyawan, Agung Tri Wijayanta, Tri Istanto	18-24			
Two-Phase Flow Characteristics On The Extensive Expansion Channel Latif Ngudi Wibawanto, Budi Santoso, Wibawa Endra Juwana	25-30			
Natural Convection Numeric Simulation On Metal Freezing Using Differential Method Heri Suprianto1, Eko Prasetyo Budiana, Purwadi Joko Widodo	31-39			
Fiber Weight Fraction Effect To Acoustic Properties Of Rhdpe Cantula Composite M. Taufik Burhany Hendrowarsito, Wijang Wisnu Raharjo, Dwi Aries Himawanto	40-43			

PREFACE

Syukur Alhamdulillah, for mercy and guidance from Allah SWT, Mechanical Engineering Scientific Magazine Volume 16 Number 2, September 2017 has been issued. Editorial boards want to say many thanks to contributors and associate editor who have provided contributions on its quality.

In this edition, journal displays 6 articles of University which represent 4 (four) of each discipline, Energy Conversion, Material/ Metallurgy and Manufacture, and Design. It begins by Muhammad Fuad Nur Rochim et al with the title "The Effect Of Cutting Fluids And Cutting Speeds To The Vibrations Of Milling Cnc Machine", Alfan Adha Hutama Putra et al with the title "Experimental Studies Of Twist Ratio Effect To The Heat Transfer Enhancement Using Square Cut Tape And Classical Tape Insert", Indra Setyawan et al with the title "Experimental Study The Effect Of Slant Angle On The Improvement Of Heat Transfer In Copper Pipe Concentric Exporter With Louvered Strip Insert Forward Structure", Latif Ngudi Wibawanto et al with the title "Two-Phase Flow Characteristics On The Extensive Expansion Channel", Heri Suprianto1et al with the title "Natural Convection Numeric Simulation On Metal Freezing Using Differential Method", M. Taufik Burhany Hendrowarsito et al with the title "Fiber Weight Fraction Effect To Acoustic Properties Of Rhdpe Cantula Composite".

We invite academician, researcher, practitioner, and professional to contribute an article in mechanical engineering field at mechanical engineering scientific magazine, which issues in March and September. Finally, we wish that these articles can be beneficially for readers, be accessible information exchange media of research result, and allocate inspiration on technology development especially mechanical engineering.

Editorial Board

THE EFFECT OF CUTTING FLUIDS AND CUTTING SPEEDS TO THE VIBRATIONS OF MILLING CNC MACHINE

A Muhammad Fuad Nur Rochim ¹, Indri Yaningsih ², Heru Sukanto ³

¹Student, ²Lecturer– Mechanical Engineering Department–Universitas Sebelas Maret

Keywords:

Milling, cutting force, cutting fluids, cutting speeds vibration

Abstract:

Vibration that occur in machining process is forced vibration. This vibration caused by external force excitation. External force that cause vibration in machining process is cutting force. This research was aims to determine the effect of cutting fluids and cutting speeds to vibration in milling process. The specimens were made using a cutting process type face milling, profile milling, pocket milling, and slot milling. Cutting speeds was variated at 62.83 m/min; 110 m/min; 157.14 m/min; 188.5 m/min. Vibration testing was done using the accelerometer sensor. Vibration response taken is the amplitude. The results show any type of cutting process has a different amplitude. Face milling has the smallest amplitude while slot milling has the biggest one. At cutting speeds parameter, the faster of cutting speeds the smaller of the amplitude. The use of cutting fluids can reduce the friction value between cutting tool and workpiece so that the cutting force will decrease. The use of cutting fluids causing the smaller the cutting force. The increase of the cutting force will cause greater vibration

INTRODUCTION

Low specific weight materials application is an effective way to reduce the structure density. Aluminum alloys are the most commonly used to substitute steel since its light weight, it also has pretty good corrosion resistance, strength, and ductility properties. The manufacturing industry was increasingly switching to aluminum as material components. In this study, aluminum 6061 was performed as the testing material. The aluminum alloys 6000 contain of silicon and magnesium that form magnesium silicide, thus making it has heattreatable capability. Although, it was powerless than most aluminum allov 2000 and 7000 series, however it became a malleable and has a medium corrosion resistance (Oberg, 2012).

An engineering company provides the production processes machineries that work manually and CNC (Computer Numerical Control). Due to its demand that must be met in the engineering field such as dimensional tolerances are very critical, CNC machine has been chosen since it has numerous advantages than manual/ conventional machine which are faster and more precisely of both quantity and quality in machining process. In this study, it was used MITSUBISHI M-70 2M-2825P CNC milling machine. The factors that affect CNC convenience compared to conventional engines were: fewer settings, the tool moves automatically by requested program, its movement can be monitored on the screen, a small error rate, and time efficiency (Zubaidi, 2012).

Aditya et al (2014) performed a study using a chisel ball nose end mill which made from carbide with conventional milling process on aluminum 6061

material. Its parameters were 700, 800, 900 rpm of spindle speed variations respectively; 100, 200, 300 mm/ min ingestion rate variations correspondingly; and were 2 and 4 chisel eye variations. Each specimen was accomplished tested a surface roughness (Ra). The results showed that feed rate has a positive influence (proportionally) that the higher feed rate, the greater surface roughness. While spindle speed and the eye chisel number have inversely effect which were the higher of them result the smaller surface roughness.

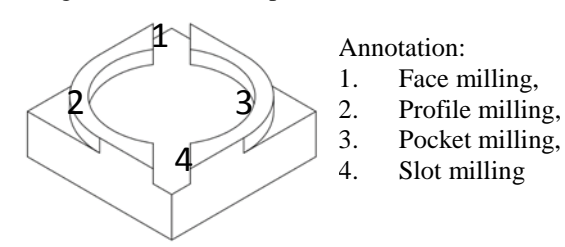
Lazuardhy et al (2012) exhibited a study by exploiting a lathe turning process that aims to determine the chatter conditions feed motion effect of the work piece surface roughness using steel S45C. This study was obtained amplitude vibrations data that occurred during the lathing process and the work piece surface roughness. The results showed that the lowest surface roughness was 0.045 mm/rev of feed motion with 5.47 lm of surface roughness value. The lowest vibration amplitudes data also produced in 0.045 mm/rev of feed motion of 121.4875 m/s². The greater feed motion will produce a force which was also affecting the higher vibration amplitude during the lathing process and will increase its work piece value.

Zhong et al (2010) completed a research on comparative studies between cutting and dry cutting process using cutting fluids based on the vibration signal. This study purpose was to examine the LQL effects (Little Quantity Lubrication) and provide effective guidance for applying LQL in machining process. This study employed an aluminum alloy 7050-T7451 with 150x 150x 45 mm of dimensions.

The utilized chisel was diamond coated flat endmill with 20 mm of diameter. The axial cut depth was 5 mm. Study parameters covered 3000, 6000, 10000, 14000, and 18000 rpm of spindle speed variations respectively. Each test was performed three treatments which were dry cutting (Cd), LOL cutting at 150ml/min (C150), and LOL cutting at 300 ml/min (C300). The vibration signal was obtained from the work piece surface. This study results indicated that the vibration signal were significantly affected by milling process cutting fluids. The dry cutting process was not only to prevent the cutting fluid exploiting, but it has a mild vibration. Meanwhile, LQL cutting process can produce a lower value of RMS vibration, machines, and chisel beneficially. The finishing was engaged LQL, which has a high quality work piece surface, but also can reduce the cutting fluids utilization in large quantities.

RESEARCH METHODOLOGY

It was using aluminum 6061 beam-shaped with 50x 50x 20mm of dimensions. The specimen chemical composition were 0.6% Si; 0.28% Cu; Mg 1.0%, and 0.20% Cr. In this study, there were four types of cutting processes (1) face milling, (2) profile milling, (3) pocket milling, (4) slot milling as can be clearly seen on Figure 1. It was applyed (63.83; 110; 157, 14; 188.5) m/min of cutting speeds, 1 mm depht of cutting, and 71 mm/min. pen feed rate.



In this study, a collected data was taken from vibration data. Its collection process at chisel was when cutting process working. It was taken using a piezoelectric accelerometer sensor that was attached to a vise, as in Figure 2. This sensor function to convert the vibration signal into electric voltage signals. Then, it forwarded to a vibration test

equipment so it displayed data which indicates a total vibration amplitude vibration of milling process system.



Figure 2. Piezoelectric Accelerometer Sensor Placement

DATA AND ANALYSIS

This study was conducted to compare the vibrations that occur during the cutting process by cutting fluids and cutting process without cutting fluids with (63.83; 110; 157.14; 188.5) m/min of spindle rotational speed cutting parameters variations. The study results was using vibration test equipment to find the vibration amplitude value of that occured during the cutting process.

Data

The aim of this test is to determine the vibration amplitude value during the cutting process. The obtained data in this test was vibration amplitude that generated by friction between the chisel eye and material. Vibrations that occur will be captured by the attached accelerometer to the vise and then forwarded to the vibration test equipment and it was obtained. The data which was taken for cutting process with and without cutting fluids, each cutting process was conducted four types of cutting (face milling, pocket milling, profile milling, slot milling, and drill) and spindle speeds variation. Each cutting process were teseted five times the yield test average are shown in Table 1.

		Vibrations (m/s²)		
Cutting Speeds	Cutting Type	Cutting Process		
		without cutting fluids	with cutting fluids	
	Face	68,57	51,78	
62,85 m/min	Profile	95,87	70,55	
	Pocket	132,39	81,76	
	Slot	248,93	239,47	
110 m/min	Face	51,29	44,46	
	Profile	91,75	62,05	
	Pocket	127,29	73,04	
	Slot	207,35	196,58	
157,14 m/min	Face	47,47	41,92	
	Profile	78,46	53,18	
	Pocket	119,50	59,18	
	Slot	198,37	184,95	
188,57 m/min	Face	38,73	33,06	
	Profile	73,89	48,35	
	Pocket	116,71	53,88	
	Slot	191,82	156,47	

Analizing The cutting speeds parameter effect to the vibrations amplitude

The vibration testing result data on Table 1 was obtained a graph of the cutting speed to vibrations amplitude relations on different cutting types as seen on Figure 3 to 6:

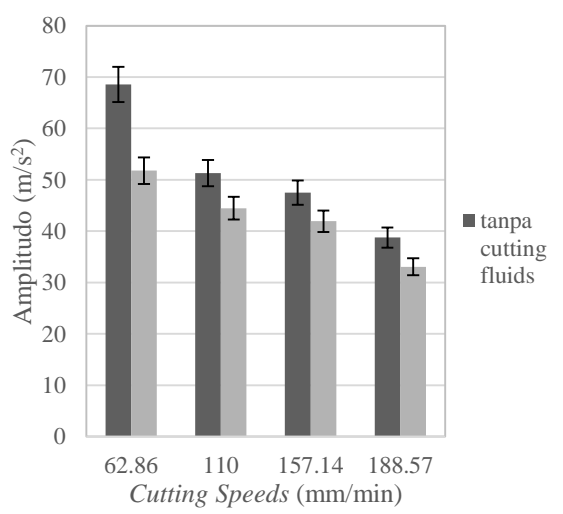


Figure 3. Graph of relationship between cutting speeds to vibration amplitude of face milling cutting style

Figure 3 shows a graph of vibration amplitude to the cutting speeds on face milling cutting type. The amount of cutting speeds gave effect to the value of the vibrations amplitude. It can be clearly seen on Figure 3, that relationship between cutting speeds to the vibrations amplitude is decreased, which each the cutting speeds addition will be decreased the vibrations amplitude. It was proved that the declining which was obtained at 62.86 m/min of cutting speeds on the face milling cutting type without cutting fluids that is equal to 68.57 m/min on the face milling cutting type without cutting fluids that is equal to 31.08 m/s².

The above phenomenon occured since cutting speeds was increased therefore cutting force will be decreased. Cutting force from this phenomenon was influenced by feed pertooth.

$$f_z = v_f/(n.z) \tag{1}$$

From the equation above feed pertooth became an important variable in the milling process and the feeding rate determined value (v_f) , spindle rotational speed (n), and the number of teeth (z). This recent study was used a chisel with the same number of 4 teeth (flute) and the same feed rate of 71 mm/min. Therefore, the main affecting factors feed pertooth was the spindle rotational speed. In this study, it was

utilizing the same cutting tool diameter of 10 mm so that the spindle rotational speed was proportional to the cutting speed. Spindle rotational speed was increasing the chisel feed pertooth speed to the work piece decreasing (Aditya, 2014). Meanwhile, the spindle rotational speed was affected by th cutting speeds value. The greater cutting speeds, the spindle rotational speed is increasing. It can be concluded that magnitude affecting the cutting speeds feed pertooth. The greater the cutting speed, the motion pertooth will be decreased.

$$F_{v} = k_{s1.1} \ h^{1-p} \ b \tag{2}$$

On Equation 2, can be seen if the feed pertooth influences on cutting forces. Based on Equation 2 in additional feed pertooth, there are other variables that affect the cut force that is specific cutting force reference (k_{s1·1}), cutting width (b), the square of average thickness chips (p), and a major cut angle (K_r). In this study, it was generating the same workpiece material was 6061, so the specific cutting force was a constant reference. This is because specific cutting force reference by workpiece tension ultimate strength was 124.1 MPa. Cutting width of this phenomenon was the same as when the slaughtering process by utilizating the same type of cuts while the independent variable were cutting speeds. It was influenced by workpiece material and cutting speed (average 0.25). While the primary cutting angle was 90°, it was because this study used a chisel end slanted tooth milling. Therefore, this phenomenon which affects the cutting forces in Equation 2 was a per tooth feeding motion. The greater it occurred then the greater the cutting force. In the previous paragraph has explained that it was affected by cutting speed. The greater cutting speeds, it value was getting down. It can be concluded the greater cutting speeds, the cutting force was getting decreased. It is convenient to the conducted research by Korkut, et al (2008) which states that the greater cutting speeds then the cutting force will be smaller.

Vibrations which occured in machining process were the forced vibration, it caused by the excitation force from the outside. Therefore, the force that produced in cutting process was influenced by vibration. In this phenomenon the forces which was act upon the milling process due to the cutting speeds repercussion were Boothoroyd cutting forces (1981), it states the greater the force exerted on the cutting process, the vibration generated amplitude will be higher. It is also supported by Budiarto et al research (2011) which states that the greater cutting force, the greater the vibration amplitude value. It can be concluded that the cutting speeds enhancement, the vibration amplitude value will be increase.

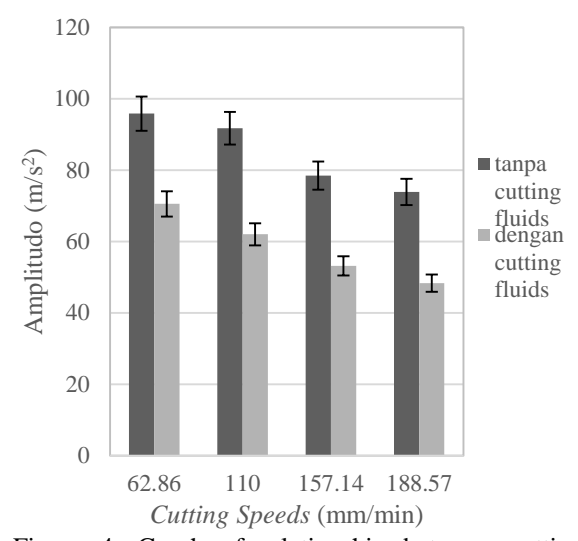


Figure 4. Graph of relationship between cutting speed and vibration amplitudo at profile milling cutting style

Figure 4 shows a graph of the cutting speeds to vibration amplitude on the profile milling cutting type. As in Figure 3 the cutting speeds value impresses of the vibration amplitude value. It can be seen on Figure 4 the cutting speeds relation to vibration amplitude is decreased, where in each cutting speeds addition it will be decreased. This decline was verified by obtained value of vibration amplitude at 62.86 m/min of cutting speeds on the milling profile cuts without cutting fluids that is equal to 95.87 m/s². While at the highest cutting speeds of 188.57 m/min on it without cutting fluids that is equal to 73.88 m/s^2 . The above phenomenon occurs because of the gained cuttting speeds make the cutting force decreased. As described in the previous paragraph cutting force on this phenomenon was influenced by feed pertooth. The higher cutting speed enhancement generates feed pertooth decreases, as a result of cutting force become smaller. The declining of cutting force value results vibration decreases.

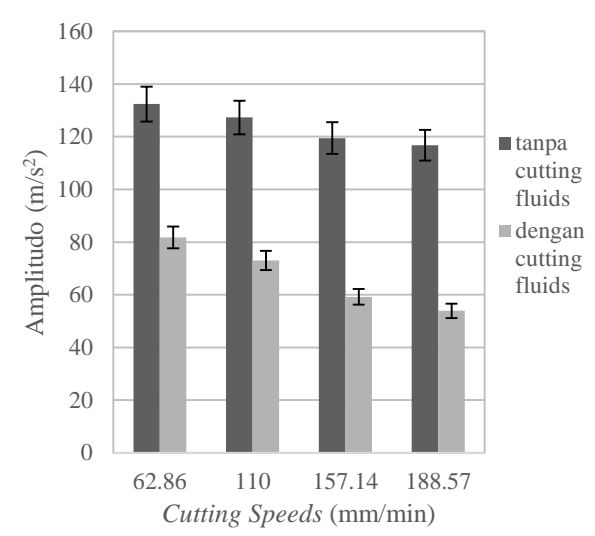


Figure 5. Graph of relationship between cutting speeds and vibration amplitudo at pocket milling cutting style

Figure 5. portrays a relation between cutting speeds and vibration amplitude graph on the pocket milling type. As in Figure 3 and Figure 4 the cutting speeds value provide an effect to vibration amplitude. It can be seen from Figure 5 the relation of cutting speeds to the vibration amplitude is weaken, with each cutting speeds addition value that will cause a vibration amplitude declined. It was illustrated by the vibration amplitude which obtained at 62.86 m/min of cutting speed on the milling slot cuts without cutting fluids that is equal to 132.39 m/s². While, at the highest cutting speeds of 188.57 m/min on the pocket milling cutting style without cutting fluids that was equal to 116.71 m/s². As described in the previous paragraph that cutting force on this phenomenon was effected by feed pertooth. The growing of feed pertooth expansion made cutting speed decreases, as a result cutting force amount getting smaller. The declining of cutting force value generates amount of vibration reduced.

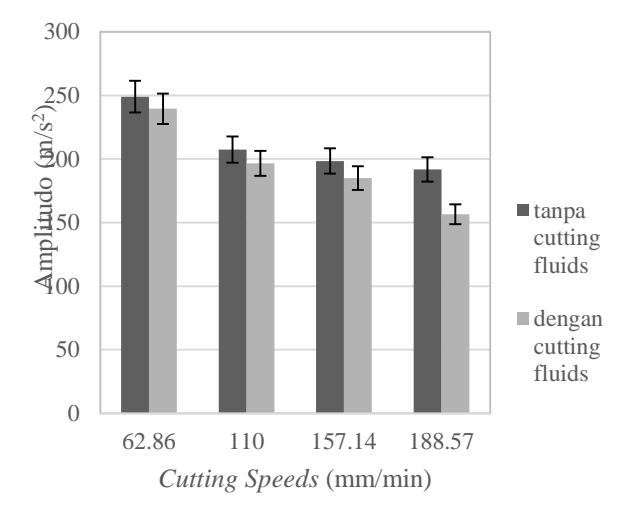


Figure 6. Graph of relationship between cutting speeds and vibration amplitudo at slot milling cutting

style

Figure 6 displays a relation of cutting speeds relationship to vibration amplitude graph on slot milling cutting style. As in Figure 3 and Figure 4 4 the cutting speeds value contribute an effect to vibration amplitude. It can be seen from Figure 6 the relation of cutting speeds to the vibration amplitude is lessen, with each cutting speeds addition value that will cause a vibration amplitude depressed. It was described by the vibration amplitude which obtained 62.86 m/min of cutting speed on the slot milling cutting style without cutting fluids that was equal to 248.93 m/s². While, at the highest cutting speeds of 188.57 m/min on the slot milling cutting style without cutting fluids that was equal to 191.82 m/s². As described in the previous paragraph that cutting force on this phenomenon was effected by feed pertooth. The growing of feed pertooth expansion made cutting speed decreases, as a result cutting force amount getting smaller. The declining of cutting force value generates amount of vibration reduced.

The cutting process effect with and without cutting fluid to the vibrations amplitude

The vibration testing data in Table 1 was obtained relation graph of cutting stlye to the vibration amplitude of cutting speeds different variations as seen on Figure 7 to 10

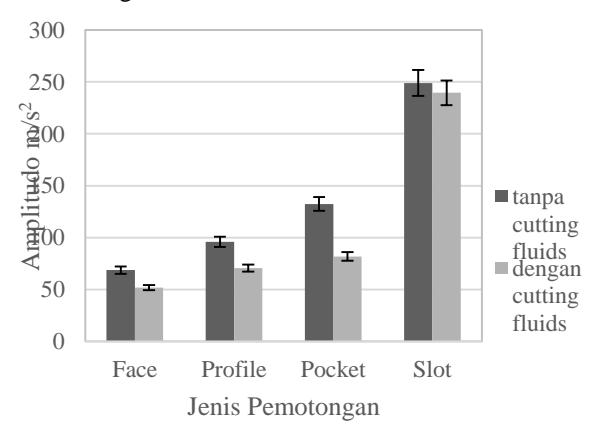


Figure 7. Graph of relationship between vibration amplitude and cutting style at 63,85 mm/min of cutting speed

Figure 7 shows a graph of relationship between vibration amplitude and cutting style at 63.85 mm/min of cutting speed. It can be clearly seen on Figure 7 that the cutting process by utilizing the cutting fluids have a greater result than without it. The difference was confirmed by vibration amplitude value which obtained in the cutting process with cutting fluids when face milling cutting style and 62.85 m/min of cutting speed was 51.78 m/s². While, in the cutting process without cutting fluids when applying face milling cutting type and 62.85 m/min of cutting speed was 68.57 m/s².

Volume 16 Number 2, September 2017

This phenomenon occurs since the cutting process with cutting fluids can reduce cutting force that emerges at machining process. It was influenced by the coefficient of friction that occurs between cutting tool to workpiece. It was convenient to the cutting fluids function which mentioned in the basic theory, where the cutting fluids applications will reduce deformation and decrease the friction between thmen therefore the cutting force would be decreased. This statement was supported by Muktiwibowo et al research (2011) which states that the cutting fluids utilizations at cutting process can reduce cutting force that appears when machining process. The forces which act on this phenomenon was used to determine the vibration amplitude that arises at the cutting process. It has been described in the preceding paragraphs, the greater the cutting force value, the higher the vibration amplitude. It can be concluded that the cutting process with cutting fluids can decrease the of the vibration amplitude value. This statement was legalized by Zhong et al research (2010) which states that the cutting process with cutting fluids can reduce vibration value compared to the process without it.

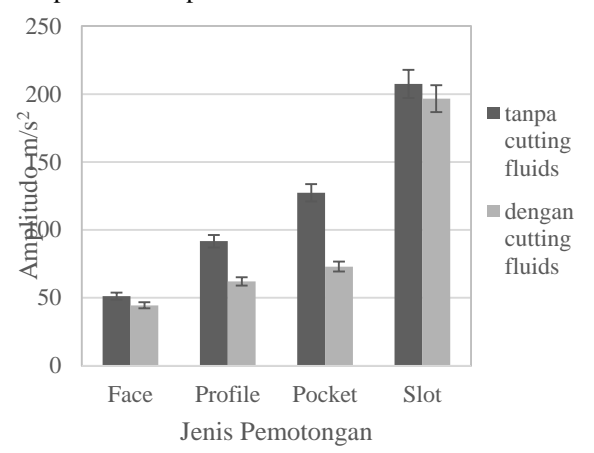


Figure 8. Graph of relationship between vibration amplitude and cutting style at 110 mm/min of cutting speed

Figure 8 displays graph of relationship between vibration amplitude and cutting style at 110 mm/min of cutting speed. It can be clearly seen on Figure 8 that the cutting process by utilizing the cutting fluids have a greater result than without it. The difference was confirmed by vibration amplitude value which obtained in the cutting process with cutting fluids when face milling cutting style and 110 m/min of cutting speed was 51.78 m/s². While, in the cutting process without cutting fluids when applying face milling cutting type and 110 m/min of cutting speed was 68.57 m/s². This phenomenon has been specified in the preceding paragraph, the cutting process with cutting fluids can scale down cutting force that exists at the machining process. Therefore, if the cutting style decline, it will develop vibrations amplitude value.

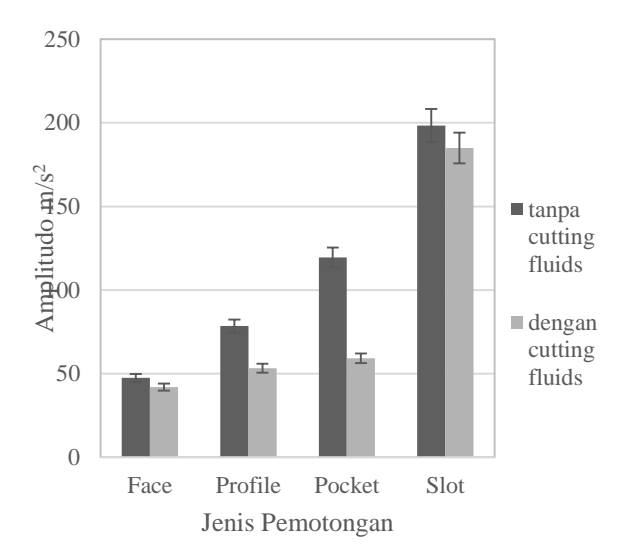


Figure 9. Graph of relationship between vibration amplitude and cutting style at 157.14 mm/min of cutting speed

Figure 9 displays Graph of relationship between vibration amplitude and cutting style at 157.14 mm/min of cutting speed. It can be clearly seen on Figure 9 that the cutting process by utilizing the cutting fluids have a greater result than without it. The difference was confirmed by vibration amplitude value which obtained in the cutting process with cutting fluids when face milling cutting style and 157.14 m/min of cutting speed was 41.92 m/s². While, in the cutting process without cutting fluids when applying face milling cutting type and 157.14 m/min of cutting speed was 47.47 m/s². This phenomenon has been illustrated in the initial paragraph, the cutting process with cutting fluids can trim cutting force that arises at the machining process. Therefore, if the cutting style fall, it will provoke vibrations amplitude value.

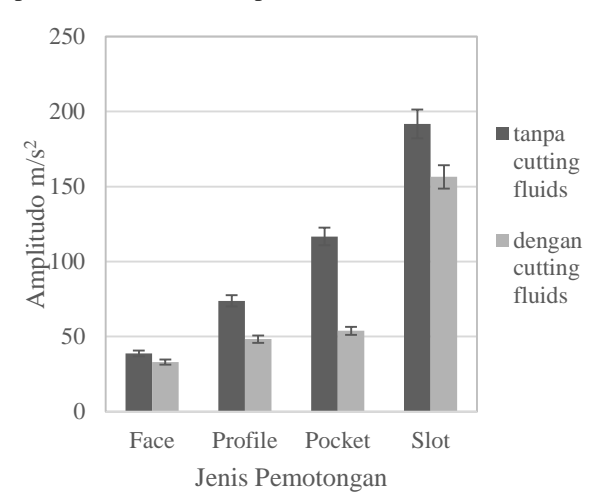


Figure 10. Graph of relationship between vibration amplitude and cutting style at 188.5 mm/min of cutting speed

Figure 10 portrays Graph of relationship between vibration amplitude and cutting style at 188.5 mm/min of cutting speed. It can be clearly seen on Figure 9 that the cutting process by utilizing the cutting fluids have a greater result than without it. The difference was confirmed by vibration amplitude value which obtained in the cutting process with cutting fluids when face milling cutting style and 188.5 m/min of cutting speed was 33.06 m/s². While, in the cutting process without cutting fluids when applying face milling cutting type and 188.5 m/min of cutting speed was 38.74 m/s². This phenomenon has been illustrated in the initial paragraph, the cutting process with cutting fluids can trim cutting force that arises at the machining process. Therefore, if the cutting style fall, it will provoke vibrations amplitude value.

The effect of cutting style to vibration amplitude

From the vibration testing result data in Table 1 was obtained a graph of relationship between cutting style and vibration amplitude at different cutting process as can be seen in Figures 11 to 12

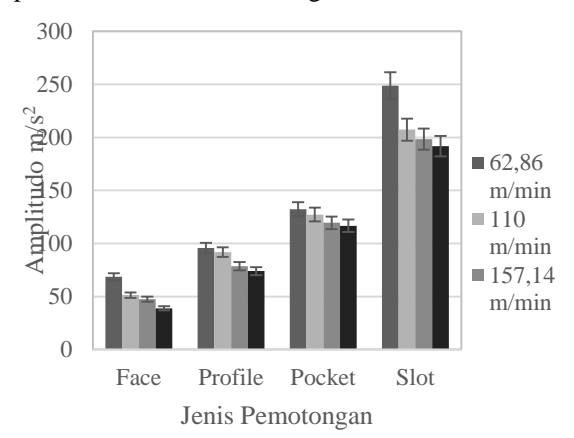


Figure 11. Graph of cutting style relationship at cutting process to vibration amplitude without cutting fluids

Figure 11 shows the current different types of cuts for cutting speed and the same cutting process will affect to the vibration amplitude value. From Figure 11 and 12 can be sorted the cutting types has the smallest amplitude value was face milling, profile milling, pocket milling, slot milling respectively. It could be justified by the magnitude of vibration amplitude values which was obtained on the face milling cutting type without cutting fluids when cutting speeds 62.83 mm/min was 68.87 m/s². Although, the slot milling cutting style without it when cutting speeds 62.83 mm/min was obtained 239.47 m/s².

The phenomenon proved that wide cutting on each cutting syle has different result. It can be seen in Figure 12.

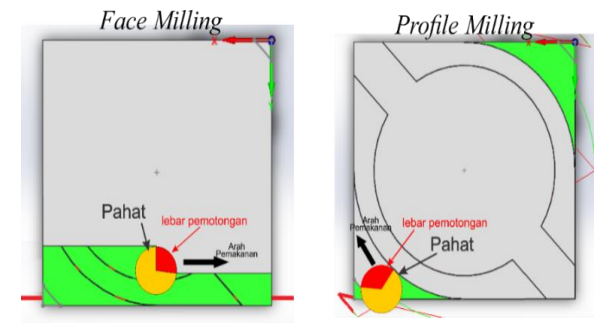


Figure 12. Cutting area at executing process

Figure 12 shows the cutting width of face milling and profile milling cutting style. In the figure 12 can be seen profile milling has a cutting width of 10.59 mm while face milling has a cutting width of 8.44 mm. Pocket milling has a cutting width which equal to the profile milling about one-third of the chisel side surface area. However, pocket milling aside from one-third of the chisel side surface area, this process also cut on the chisel face side. Therefore, the pocket milling cutting style has a cutting width greater than profile milling cutting style. The slot milling cutting style has a cutting width of a half surface area of the side chisel and also trim on the chisel face side. Thus, slot milling cutting style has a cutting width is greater than other types of cuts.

Cutting width is directly proportional to the imposed cutting force on the workpiece (Lazuardhy, 2012). The force which was generated from cutting process by chisel produced a vibration. It will grow up as the cutting forces is generated. The greater the cutting forces exhibited, the higher vibration will be created (Boothoroyd, 1981). Therefore, if the cutting force is establishing a smaller value, the amplitude is also getting smaller.

Pocket milling cutting style has a vibration amplitude value which was greater than other profile milling cutting style. Both these processes were using an end mill chisel with the same diameter of 10 mm, 71 mm/min of feeding rate, and 1 mm of feeding thickness. The main factors that affect the vibration amplitude vibration value was cutting forces when executing. The pocket milling and profile milling cutting style were exploited the same parameters and cutting distinguishing factor was the cutting width. The bigger the cutting width, the cutting forces will also rise up (Rochim, 1993). The profile milling and pocket milling cutting style had the same cutting width which was about one-third of the side surface area of the pocket milling chisel but in addition to one-third of the chisel side surface area, this process also cut off the chisel face side. The pocket milling cutting have cutting width larger than profile milling. It can lead pocket milling has a huge vibration amplitude.

The slot milling cutting style has the greatest vibration amplitude value. It caused by the vibration amplitude value greater than the both previous cutting process was cutting width difference as described in the preceding paragraph. The slot milling cutting style has a cutting width which half side surface area of chisel and also trim on the chisel face side. It has a cutting width greater than the pocket milling cutting process which is why the slot milling cutting process has greatre value of vibration amplitude.

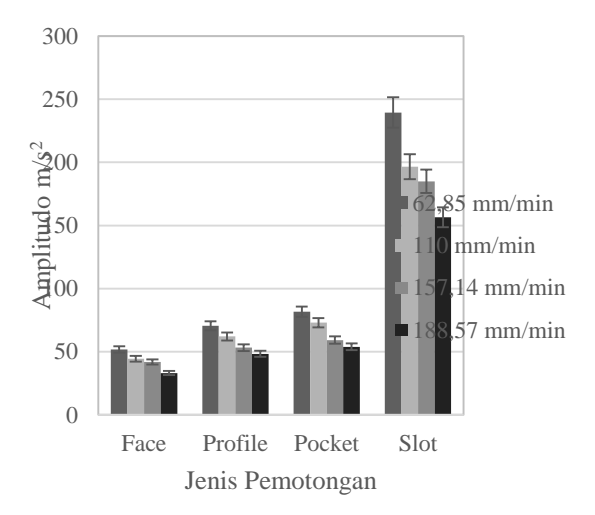


Figure 13. Graph of relationship between vibration amplitude value on cutting process with cutting fluids

Figure 13 shows a graph of relationship between vibration amplitude value to the cutting style on cutting process with cutting fluids. It can be seen that the amplitude value of face milling is smaller than other types of cuts. This phenomenon has been described in the preceding paragraph which is voiced that face milling cutting has a cutting width smaller than other styles. While slot milling has greatest cutting width so the amplitude value is getting high. It can be concluded that the greater cutting width, the larger the amplitude value which was generated during the cutting process.

CONCLUSION

From the data analysis and discussion can achieve several conclusions as follows:

- Vibration of any kind of cutting style, the smallest value were face milling, profile milling, pocket milling, and slot milling respectively.
- 2. At 62.83 m/min of cutting speed has the largest vibration amplitude of vibration cutting speed while at 188.57 m/min has the smallest.
- The cutting process with cutting fluids will result the coefficient of friction that occurs in machining process was more and more go down when compared to the cutting process without cutting fluids. It caused a lessen vibrations.

REFERENCE

- Aditya, A. Y., Sonief, A. A., & Raharjo, R. (2014).

 Pengaruh Spindle Speed, Feed Rate dan
 Jumlah Mata Pahat Ball Nose End Mill
 Terhadap Kekasaran Permukaan
 Aluminium Pada Proses Conventional
 Milling. Malang.
- Aguiar, M., Anselmo, E. D., & Pederiva, R. (2013). Correlating surface roughness, tool wear and tool vibration in the milling process of hardened steel using long slender tools. Brazil: International Journal of Machine Tools & Manufacture 68 (2013) 1–10.
- Boothroyd, G. (1981). Fundamentals of Metal Machining and Machine Tools. Washington D.C: Scripta Book Company.
- Budiarto, W., Sutikno, E., & Sulistyo, E. (2011).

 Pengaruh *Cutting Speed* dan *Depth of Cut*Kondisi *Chatter* Terhadap Kekasaran

 Permukaan Benda Kerja Proses Bubut.

 Malang.
- Ihsan, K., & Mehmet, B. (2008). Experimental Examination of Main Cutting Force and Surface Roughness Depending on Cutting Parameters. Turkey: Journal of Mechanical Engineering 54(2008)7-8, 531-538.
- Lazuardhy, M. T., Sutikno, E., & Sulistyo, E. (2012).

 Pengaruh *Feed Motion* Kondisi *Chatter*Terhadap Kekasaran Permukaan Benda
 Kerja Proses Bubut. Malang.
- Muktiwibowo, S., Sutikno, E., & Oerbandono, T. (2011). Pengaruh *Depth Of Cut* dan Variasi *Cutting Fluid* Terhadap *Surface Roughness* Aluminium 6061 Hasil Proses Turning. Malang.
- Nugroho, T. U., Saputro, H., & Estriyanto, Y. (2012). Pengaruh Kecepatan Pemakanan dan Waktu Pemberian Pendingin Terhadap Tingkat Keausan *Cutter End Mill HSS* Hasil Pemesinan CNC *Milling* Pada Baja St 40. Surakarta: Universitas Sebelas Maret.
- Rawangwong, S., Chatthong, J., Boonchouytan, W., & Burapa, R. (2014). Influence of Cutting Parameters in Face Milling Semi-Solid AA 7075 Using Carbide Tool Affected the Surface Roughness and Tool Wear. Thailand: Energy Procedia 56 (2014) 448 457
- Rochim, T. (1993). Teori & Teknologi Proses Permesinan. Bandung: ITB.
- Sugondo, A., Siahaan, I. H., & Kristanto, B. (2008). Studi Pengaruh Kedalaman Pemakanan terhadap Getaran dengan Menggunakan Mesin Bubut *Chien Yeh CY 800 Gf.* Bandung.
- Thomson, William T. (1995). Teori Getaran Dengan Penerapan. Terjemahan Lea Prasetio. Jakarta: Airlangga.
- Zhong, W., Zhao, D., & Wang, X. (2010). A comparative study on dry milling and little

MEKANIKA 9 Volume 16 Number 2, September 2017

quantity lubricant milling based on vibration signals. China: International Journal of Machine Tools & Manufacture 50 (2010) 1057–1064.

EXPERIMENTAL STUDIES OF TWIST RATIO EFFECT TO THE HEAT TRANSFER ENHANCEMENT USING SOUARE CUT TAPE AND CLASSICAL TAPE INSERT

Alfan Adha Hutama Putra¹, Agung Tri Wijayanta ², Indri Yaningsih ³ ¹Student, ²Lecturer– Mechanical Engineering Department–Universitas Sebelas Maret

Keywords:

Square cut tape insert Friction factor Heat exchanger Nusselt number Twist ratio

Abstract:

This research was conducted experimentally to examine the effect twist ratio on heat transfer enhancement in the concentric tube heat exchanger with the addition of square cut and classical cut tape insert. Test section was the single pass concentric tube heat exchanger with inner tube and outer tube made of aluminum. Flows in the inner tube and in annulus were counter flow. Working fluid in the inner tube was hot water which its inlet temperature was maintained at 60°C, whereas the working fluid in the annulus was cold water. square cut and classical cut tape insert tape insert with the twist ratio (Y) variation = 2,7; 4,5; and 6,5 installed in the inner tube of the concentric tube heat exchanger. Research's result shown that heat transfer enhancement in the concentric pipe with augmentation at the same Reynolds number, the addition of square cut and classical cut tape insert with the twist ratio (Y) = 2,7; 4,5;and 6,5 into the inner tube increase the Nusselt numbers has been 79%; 58,2%; 43,5% and 67,8%; 48,7%, 31,1% compared to the plain tube, respectively. At the same Reynolds number, the addition of square cut and classical cut tape insert with the twist ratio (Y) = 2.7; 4.5; and 6.5 into inner tube has produced an friction factor 2,58%; 2,2%; 1,74% dan 2,41%; 1,96%, 1,44% than the friction factor of plain tube, respectively. The addition of square cut and classical cut tape insert with the twist ratio (Y) = 2,7; 4,5; and 6,5 into the inner tube has produced an enhancement heat transfer ratio of 1,3; 1,2; 1,1; and 1,23; 1,1; 1,1, respectively.

INTRODUCTION

Heat transfer enhancement techniques, especially in heat exchanger, can substantially improve its performance. The general objective of this technique is to reduce the heat exchanger size, increase its capacity, and cut down heat exchanger pumping power. It can be classified into three groups; techniques of passive, active, and mix. Its passively technique is acquired without providing additional energy flow. The active one is conducted by providing extra energy to the fluid flow, so that the active technique requires higher costs than passive techniques. In a mix of techniques, two or more of the active and passive techniques are used generate simultaneously to heat transfer enhancement, where it is higher than other techniques which are operated separately.

Twisted tape inserts is one of the techniques which practiced to boost a passively heat transfer on heat exchanger. It became most popular due to their low cost and easy installation. On the other hand, twisted tape inserts which purposed as a continuous flow twisting device to enhance the heat transfer rate.

Research on heat transfer enhancement of heat exchanger has ever performed by employing inserts with v-cut punched and twisted tapes. Test section has 700 mm of display dimension, 26 mm of inner

diameter, 30 mm of outside diameter, 2 mm of thickness. Punched and v-cut twisted tapes operated variations in 9, 10, and 11 of twist ratio. The results portrayed that its heat transfer rising in comparison with the plaint tube from 3.34 to 14.4% for 9 of twist ratio and 13.35 to 25% with a twist ratio of 11. Its maximum friction factor was 52% at 9 of twist ratio and 66% at 11 of twisted ratio that compared with plain tube. (Quazi and Mohite-2015).

Previously, also conducted an experimental research on heat transfer characteristics, friction factor, and thermal performance of turbulent flow in a round pipe with a rectangular-cut twisted tape insert. Twisted tape was made of stainless steel with 2 mm of thickness and 20 mm of width, 105 mm of length so the twist pitch ratio was 5.25. The results displayed that at the same Reynolds number, Nusselt number in rectangular-cut pipe with twisted tape inserts roses 2.3 to 2.9 compared with plain tube, with the average expansion of 2.6 times. The pipe friction factor for a rectangular-cut twisted tape insert were 39% to 80% higher than the plain tube friction factor. The thermal performance ranges were from 1.9 to 2.3. (Salam, et al 2013).

The experimental study on heat transfer characteristics of a heat exchanger with Elliptical-cut twisted tape insert on twist ratio (y= 8.0) and five ratio of major to minor (Z) were 5; 4; 3.3; 3, and 2.5.

The Reynolds number variations of 10000-19000, 14-22kw/ m² of heat flux variations on a plain tube and 23-40 kW/ m2 for inserted pipes. The results exhibited that the Nusselt numbers average was rised with the increasing number of Z = 5; 4; 3.3; 3, and 2.5 at 19.3%; 41.8%; 53.83%; 68.5%; 73.16%; and 84.5% respectively, it were higher compared to the plain tube. The performance of thermally-cut elliptical twisted tapes ranges from 0.91 to 1.25 for Z = 5.0; 4.0; 3.3; 3 and 2.5. (Ganorkar, et.al-2015)

This study was conducted to examine the effect of the Reynolds number variations and the effect of adding squere-cut twisted tape insert in the pipe in the (inner tube) on the heat exchanger pipe concentric annular channel on the characteristics of heat transfer and friction factor. It is expected with the addition of inserts squere-cut twisted tape inserts and twisted tape insert with a classical twist variation ratio can improve convection heat transfer coefficient of heat exchanger pipe in pipe concentric with the increase in pressure drop is acceptable.

RESEARCH METHODOLOGY

Testing Equipment and Research Procedure

Research equipments consist of three systems, such as, the hot water flow system tracks in the pipes, measurement, and path of the cold water flow in the annulus. The electric water heater with a total power of 4,000 watts was employed to heat the water in the hot water tank. On it, the hot water temperature was setup using thermocontroller to keep constant at 60°C to the hot water pipes temperature enter through inside of the concentric pipe heat exchanger. The water heat pumps for pumping hot water from the hot water tank, passing through heat exchanger test equipment and then hot water returned to the hot water tank. The testing equipment scheme can be seen in Figure 1. The fluid flow direction on the pipe and the annulus were in opposite directions.

Bypass valve was used to regulate water flow variations in the amount of heat water which entering the pipe and it values can be read with a rotameter. Cold water which flowing into the annular was constantly maintained during the test. It flowing by gravity method was the cold water flow which coming from the cold water tank that located above the cold water surface elevation in the cold water tank to keep constant by employing the overflow pipe. The cold water that comes out of the test equipment heat exchanger immediately discarded.

The U shape Manometer was employed to measure the pressure difference on the hot water which flowing at a side entrance and the exit. Water was used inside manometer. Trapped water was used to store the water-borne upon the manometer pressure measurement in order not to get into the

The temperature measurement of the cold water at in and out annular, outer wall temperature and the hot water temperature in the pipe at in and out was type thermocouple temperature measurement of the outer walls of the pipes which totaling 10 points that measured alternately. Thermocouple reader was exploited to read the thermocouple. The U pipe manometer fluid with water was used in measurement of the pressure drop in the pipeline. A concentric heat exchanger pipe with a one pass pipe was made of aluminum. The dimensions of the concentric pipe heat exchanger can be seen in Figure 2.

Square cut twisted tape inserts and classical tape inserts nomenclature in a pipe can be seen in Figure 3. In Figure 3, W is thick, y is the pitch square cut twisted tape insert, d is the cutting height, W is the width (twist). In the previous research the inside part of pipe was made of aluminum with 25 mm of inner diameter and 2000 mm of length. Twisted tape inserts made of aluminum with 1.5 mm of thickness and 23.5 mm of width. Plain twisted tape insert and a square-cut twisted tape which used has a twist ratio of 2.0; 4.4; and 6.0 (Murugesan, et al., 2010).

A flow Reynolds number of water in the pipe was varied by adjusting the flow rate of 2-6 LPM to pipe in without STT (plain tube) and inner pipes with STT. Data was obtained by the inlet and outlet water temperature of annulus, outer wall temperature, the water mass flow rate, and the annulus pressure drop in the pipeline. For each test variation data was collected every 10 minutes to obtain a steady state. The data of these steady state conditions were used in the research data computation and analysis. For comparison, there was performed testing on the pipeline without STT (plain tube) and with the square-cut tape inserts addition and classical twisted tape insert.

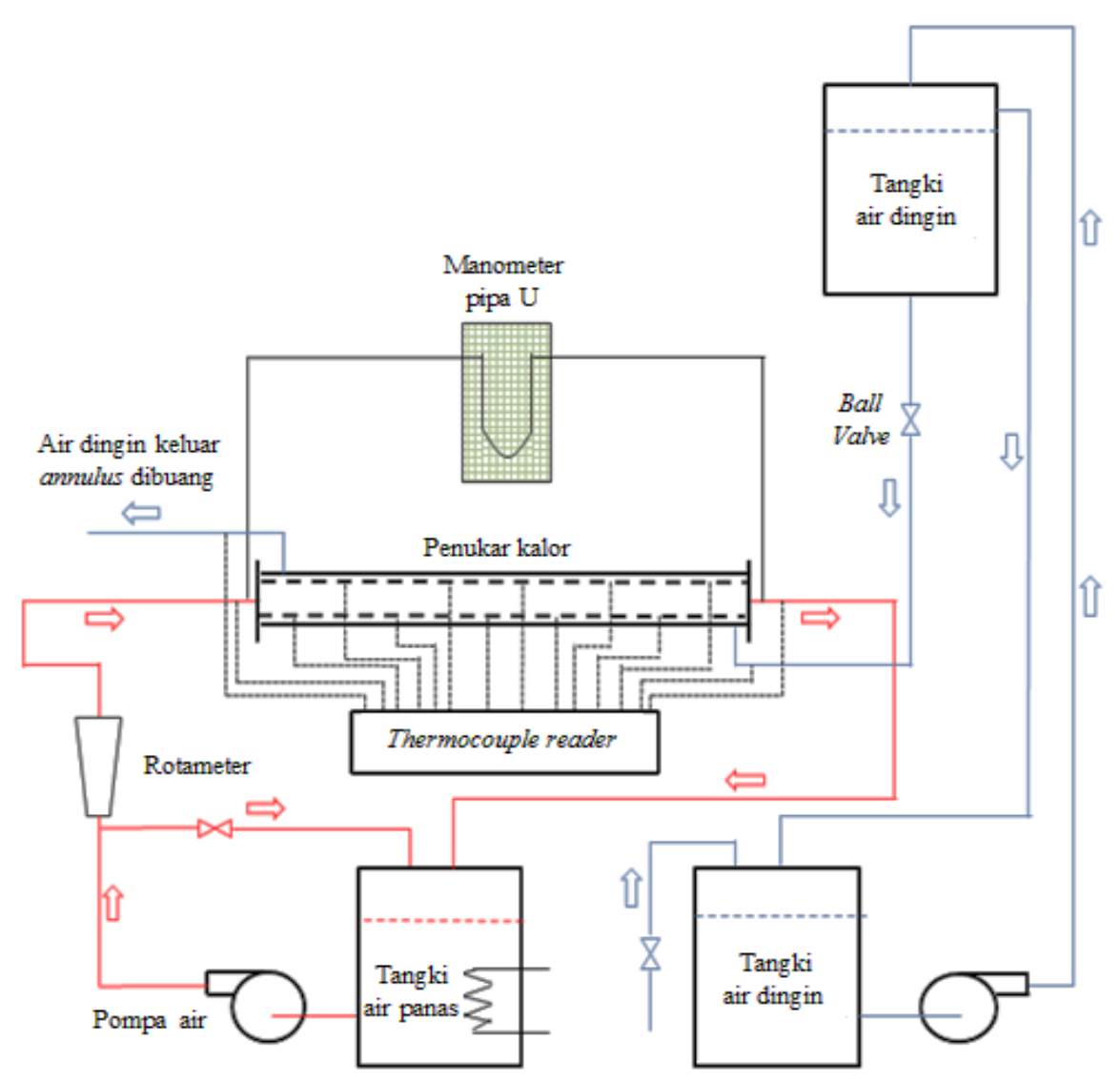


Figure 1. Concentric pipe heat exchanger scheme by square-cut twisted tape insert.

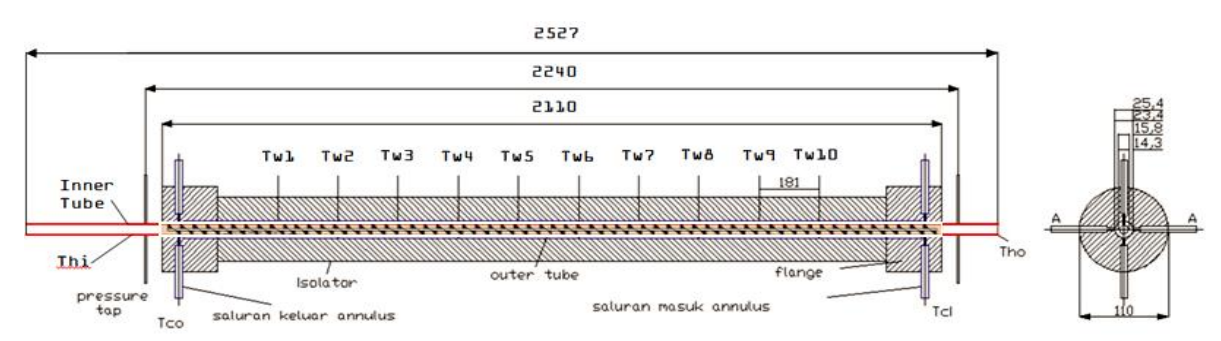


Figure 2. Concentric pipe heat exchanger scheme

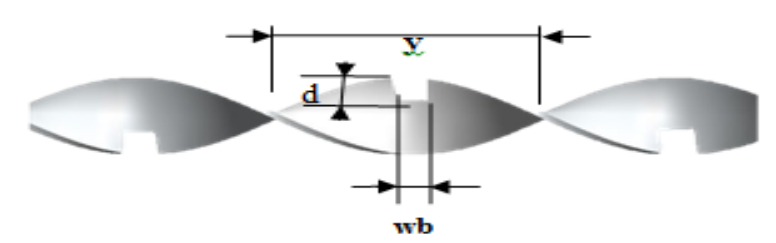


Figure 3. Length square-cut twisted tape insert nomenklatur on a pipe

Characteristic Calculation, Friction Factor, and **Increasing Ratio** of Heat Exchanger **Concentric Pipe**

Heat transfer rate on innert tube can be stated as formula (1):

$$Q_{h} = m.C_{p,h}.(T_{h,i} - T_{h,o}) = U_{i}A_{i}\Delta T_{LMTD}$$
 (1)

Heat transfer rate to cold water on the annulus side could be defined as following formula (2):

$$Q_{c} = \stackrel{\cdot}{m}.C_{p,c}.(T_{c,o} - T_{c,i}) = h_{o}.A_{o}.(\overline{T}_{w,o} - T_{b,c}) (2)$$

In which to define bulk temperature on concentric inner pipe as this following formula (3):

$$T_{b,c} = \frac{T_{c,i} + T_{c,o}}{2} \operatorname{dan} \overline{T}_{w,o} = \frac{\sum_{i=1}^{i=10} T_{w,i}}{10}$$
(3)

Heat loss percentage (% Q_{loss}) could be defined as following formula (4):

Overall heat transfer coefficient based on surface area on innert tube which could be defined as formula (5):

$$U_i = \frac{Q_h}{A_i \ \Delta T_{LMTD}}$$
(5)

In which a counter flow heat exchanger ΔT_{LMTD} number could be defined as formula (6):

$$\Delta T_{LMTD} = \frac{\Delta T_2 - \Delta T_1}{\ln \left(\Delta T_2 / \Delta T_1 \right)} = \frac{\Delta T_1 - \Delta T_2}{\ln \left(\Delta T_1 / \Delta T_2 \right)}$$
where $\Delta T_1 = (T_{hi} - T_{co})$ and $\Delta T_2 = (T_{ho} - T_{co})$. (6)

Median of convection heat transfer coefficient on the annulus side could be defined by this following formula (7):

$$h_o = \frac{Q_c}{A_o \left(\overline{T}_{w,o} - T_{b,c}\right)} \tag{7}$$

Median of convection heat transfer coefficient on the innert tube side could be defined by this following formula (8):

$$\frac{1}{U_i A_i} = R_{total} \tag{8}$$

Then, to define innert tube overall heat exchanger by formula (9):

$$\frac{1}{U_{i}.A_{1}} = \frac{1}{h_{i}.A_{i}} + \frac{\ln\left(d_{o}/d_{i}\right)}{2\pi k_{p}L} + \frac{1}{h_{o}.A_{o}}$$
(9)

where

$$A_i = \pi.d_i. L$$

 $A_o = \pi.d_o. L$

Therefore, median of convection heat transfer coefficient on the innert tube side could be defined as following formula (10):

$$h_{i} = \frac{1}{\left[\frac{1}{U_{i}} - \frac{d_{i} \cdot \ln(d_{o}/d_{i})}{2k_{p}} - \frac{d_{i}}{d_{o} \cdot h_{o}}\right]}$$
(10)

An average Nusselt number on the innert tube side could be defined as this following formula (11):

$$Nu_i = \frac{h_i . d_i}{k_{fi}} \tag{11}$$

Heat exchanger effectiveness could be defined as following formula (12):

$$\varepsilon = \frac{Q_{aktual}}{Q_{maksimum}} = \frac{Q_h}{C_{\min} \cdot (T_{h,i} - T_{c,i})}$$
(12)

pressure drop of innert tube could be defined as following formula (13):

$$\Delta P = \rho_{\rm m} \cdot g \cdot \Delta h$$
 (13)

Pumping power could be defined as following formula (14):

$$W_{\text{pompa}} = \stackrel{\bullet}{V} . \Delta P \tag{14}$$

Friction factor on the innert tube side could be defined as this following formula (15) berikut ini::

$$f = \frac{\Delta P}{\left(\frac{L_t}{d_i}\right)\left(\frac{\rho \cdot V^2}{2}\right)} \tag{15}$$

Reynolds number of hot water flow on the innert tube side could be defined as this following formula (16):

$$Re = \frac{\rho . V. d_i}{\mu} \tag{16}$$

where of the hot water on innert tubes properties (ρ , kfi, dan μ) was evaluated by average bulk hot water temperature (Tb, h).

Heat transfer enhancement ratio factor at constant pumping power is the comparison of average convection heat transfer coefficient ratio of the innert tube in with a plain tube inserts which can be written by equation (17) below:

$$\eta = \frac{h_s}{h_p} \bigg|_{pp}$$
(17)

Heat transfer characteristics, friction factor, and heat transfer enhancement ratio can be expressed in a row with a graph of Nu to Re, f to Re, and η to Re.

Heat transfer characteristics validation on insert pipe without plain tube inserts using (18) Distus - boelter and Gnielinski equation:

$$Nu = \frac{(f/8) \cdot Re \cdot Pr}{1,07 + 12,7 \cdot (f/8)^{1/2} \cdot (Pr^{2/3} - 1)}$$
(18)

Petukhov formula (20) was applied for fully developed and number of $0.5 \le Pr \le 2000$ and 10^4 <Re<5x10⁶.

Gnielinski equation(19):

$$Nu = \frac{(f/8).(Re-1000).Pr}{1+12.7.(f/8)^{1/2}.(Pr^{2/3}-1)}$$
(19)

Gnielinski equation (19) was applied for fully developed and number of 0.5≤Pr≤2000 and 10^3 <Re< $5x10^6$. On (18) dan (19) equation, friction factor number (f) could be defined as following formula (20):

$$f = (0.790 \ln \text{Re} - 1.64)^{-2}$$
 (20)

Heat transfer characteristics validation on insert pipe without plain tube inserts as following Blasius equation (21):

$$f = 0.3164.\text{Re}^{-0.25}$$
 (21)

Blasius equation (21) for number of $4 \times 10^3 < \text{Re} < 10^5$.

RESULT DAN DISCUSION a. Plain Tube Validation

In this research, heat transfer characteristics validation for a plain tube was demonstrated by Gnielinski and Dittus- Boelter empirical correlations. Figure 4 below shows Nu_i to Re correlation on a plain tube.

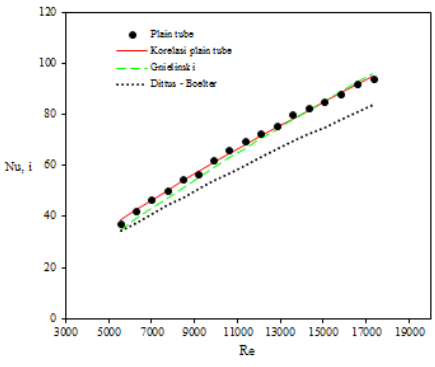


Figure 4. Nui to Re correlation on a plain tube graph

Figure 4 shows the average deviation of plain tube friction factor correlations to Dittus-boelter and Gnielinski, 13.8% and 3.4% respectively. Average deviation of Nui plain tube to Gnielinski and Dittusboelter the correlations were less than 10% and 25%. ON actual plain tube average deviation to Dittus-Boelter correlation of 13.8%, Gnelienski by 3.4%, while the plain tube correlation of about 1.8%. There was an average deviation value which compared with Nu Gnielinski correlation, Dittus-Boelter correlation, and plain tube were still small enough, therefore the obtained data to Nu number on innert tube of the concentric pipe heat exchanger without twisted tape inserts, plain tube was valid. In this study also were validated friction characteristics of the plain tube by using Blasius empirical correlations. Characteristics of plain tube friction factor and innert tube friction factor (f) can be seen in Figure 5 below.

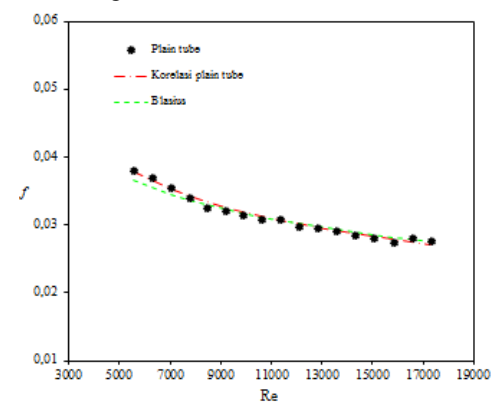


Figure 5. f to Re correlation on plain tube graph

Figure 4-5 shows a comparison between Nu_i and f to plain tube which compared to the empirical correlation calculation results. Deviations of plain tube Nusselt numbers against empirical Gnielinski and Dittus-consecutive boelter correlation were less than $\pm 4.1\%$ and $\pm 13.4\%$. Whereas, deviation of the plain tube friction factor correlation was \pm 1.8%.

b. Twist Ratio Effect to Heat Transfer of Heat **Exchanger Characteristics with Square Cut** Tape Insert and Classical Tape Insert.

Heat transfer characteristics of the heat exchanger tube in the concentric pipe can be seen in Figure 6.

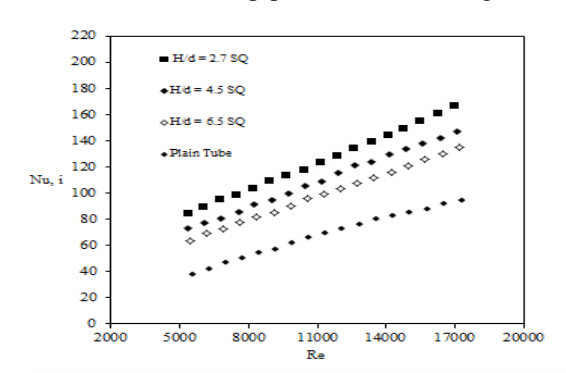


Figure 6. Nu_i to Re correlation graph

Figure 6 portrays that the larger Reynolds number, average Nusselt number (Nu_i) were increasing. It was met a plain tube or innert tube with square cut tape inserts and classical tape insert. Extra inserts square cut tape insert made Nui on innert tube larger than Nu_i plain tube. It proves that cut tape innert square inserts can increase the convection tube heat transfer rate. Extra square cut tape inserts caused the fluid flow turbulence intensity which passing through the tube wall was greater. It was

generating the fluid mixing very well which resulting in an increased heat transfer (Murugesan, 2010).

The greater the twist ratio, pipe Nu_i will be decreased. It was caused by the greater twist ratio, to decrease the turbulence flow intensity on innert tube and also fluid dwell time becomes faster which causes Nui decreased. In Figure 6, the testing results showed that 5.400 < Re < 17.500, the average Nusselt number (Nu_i) on innert tube with square cut tape insert for twist ratio variations of 2.7; 4.5; and 6.5 successively increased in 79%; 58.2%; 43.5% which compared to the plain tube.

c. Twist Ratio Effect to Friction Factor Characteristic and Square Cut Tape Insert dan Classical Tape Insert Heat Exchanger

The pressure drop comparison characteristics between the plain tubes and square cut classical twisted twisted tape and tape were completed. In Figure 7 below shows Re to a pressure drop correlation at each variations.

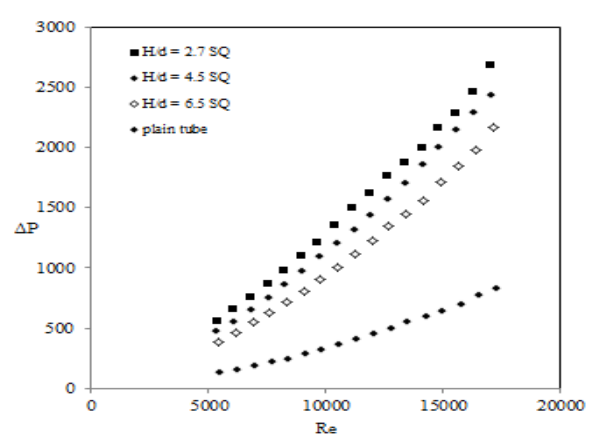


Figure 7. ΔP to Re correlation graph

Reynolds number of 5.400<Re<17,500 with a smaller twist ratio, the greater pressure drop on innert tube will occur. This could be originated due to the narrower twist ratio, the larger contact surface area and greater flow obstruction which causing a higher pressure loss. Average pressure drop on innert tube of inserts square inserts with cut tape twist ratio of 2.7; 4.5; and 6.5 were 2.41%; 1.96%, 1.44% respectively, greater than the pressure drop across the plain tube.

d. Twist Ratio Effect to Heat Exchanger Friction Factor Characteristic of Square Cut Tape Insert and Classical Tape Insert.

Friction factor characteristics with of square cut tape insert twist variations ratio of 2.7; 4.5; and 6.5 on innert tube of the concentric pipe heat exchanger can be seen in Figure 8. The larger the Reynolds number, the friction factor decreases both in plain tube or square cut tape insert. It was caused by the higher Reynolds number, the water flow rate on it will further increase as the friction factor was inversely

proportional to its water flow squared velocity. Friction factor value on innert tube of square cut tape insert has a greater value than the plain tube. Furthermore, to recognize the friction factor to STT and CTT numbers correlation is shown in Figure 8 below.

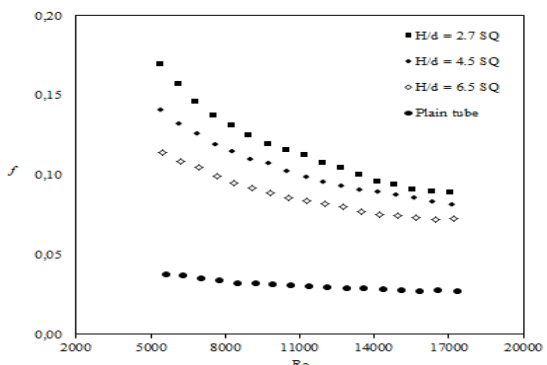


Figure 8. f to Re correlation graph

Figure 8 displays that the square cut tape insert with a smaller twist ratio, the greater friction factor. It may be caused by small twist ratio geometry and larger surface area to reduce the fluid free flow, which causing friction between the insert and the pipe wall getting larger (Suresh, 2012). In 5.300<Re<17.500 he friction factor was boosted on innert pipe of inserts square inserts with a cut tape twist ratio variations of 2.7; 4.5; and 6.5 were 2.58; 2.22; 1.73 respectively which is greater than the friction factor on a plain tube.

e. Twist Ratio Effect to Ratio Characteristic of Heat Transfer Enhancement of Heat Exchanger of Helical Screw Tape Insert

Extra inserts Square cut tape inserts provide variations in twist ratio affect the ratio of the heat exchanger with a pumping power enhancement. Figure 10 below shows the pumping power efficiency to Reynold number correlation.

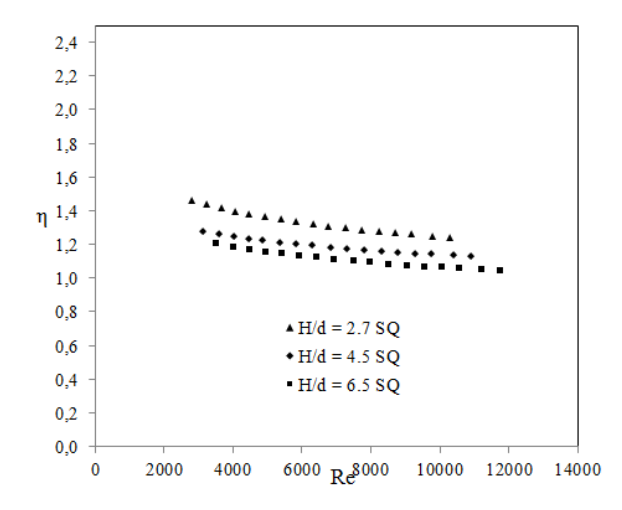


Figure 10. η dengan Re correlation graph

Figure 10 shows that the heat transfer enhancement ratio on innert tube which getting up to

twist ratio was getting smaller due to the fluid turbulence flow which larger along with the lack of twist ratio. It portrays that the square cut tape insert with a twist ratio less storing energy capable of given operating condition. Figure 10 exhibits that adding effect of square inserts cut tape and innert tube into the heat transfer rate was a significantly improved.

Heat transfer enhancement ratio of heat exchanger of square cut tape inserts 2.7; 4.5; and 6.5 were 1.3; 1.2; 1.1 respectively. It means that at the same pumping power, convection heat transfer average coefficient value of the tube of square cut tape insert was greater than the convection heat transfer average coefficient on plain tube.It was appropriated to research (Murugesan, 2009).

CONCLUSION

Based on the testing results, analysis, and discussion by the previous chapter about the heat transfer and friction factor characteristics of the heat exchanger concentric pipe of square cute twist tape insert with 2.7, 4.5, and 6.5 of variations ratio can be concluded as follows:

- The square cut tape inserts in 5500<Re<17500, has a Nu_i value, 79%; 58.2%; 43.5% respectively which compared to the plain tube. The friction factor of 2.58%; 2.22%; 1.73% and the heat transfer enhancement ratio of 1.3; 1.2; 1.1 times were larger than the plain tube.
- The heat transfer characteristics, the friction factor, and a leverage ratio of twisted tape inserts heat was increased along the little twist ratio than without plain tube inserts.
- A range of 5.500<Re<17.500 square cut tape insert has heat transfer characteristics value. friction factor, and heat transfer enhancement ratio was higher than the classical twisted tape.

NOMENKLATUR

= channel surface area (m²) A_{c}

 A_{i} = inner pipe surface area (m²) = inner pipe external surface area (m²) A_{o}

= cold water spesific heat (kJ/kg.°C) $C_{p,c}$ $C_{\text{p},\text{h}}$ = hot water spesific heat (kJ/kg.°C)

= inner pipe diameter d_i

= inner pipe external diameter d_{o}

D = pipe diameter (m) f = friction factor

= plain tube friction factor f_p = insertion pipe friction factor f_s

= gravity (m/s^2) g

h = convection heat transfer coefficient inner pipe average (W/m².°C)

= convection heat transfer coefficient h_0 at annulus average (W/m².°C)

= convection heat transfer coefficient of h_{p} average inner pipe without twisted tape insert (W/m².°C)

h, = convection heat transfer coefficient average inner pipe with inserts (W/m².°C)

= the average thermal conductivity of inner k_i pipe hot water (W/m.°C)

= thermal conductivity of deep pipe k_p material (W/m.°C)

= pressure drop measurement length of L_{t} inner pipe (m)

 \dot{m}_c = cold water mass flow rate (kg/s) = hot water mass flow rate (kg/s) \dot{m}_h

= average inner pipe Nusselt number Nu_{i} = the average Nusselt number of plain tube Nu_{p} = the average Nusselt number inner pipe Nu_n

using inserts = equal pumping power pp

Pr = Prandtl number

= actual heat transfer rate of heat exchanger Q_{aktual}

 Q_c = annulus heat transfer rate (W) = inner pipe heat transfer rate (W) Q_h Q_{loss} = inner pipe heat loss convection (W)

 $Q_{maksimum}$ = maximum heat transfer rate Probably from a heat exchanger (W)

Re = Reynolds number

= average bulk temperature at annulus (°C) $T_{b,c}$ = average inner pipe bulk temperature (°C) $T_{b,h}$ = cold water temperatures enter the annulus $T_{c,in}$

 $T_{c,out}$ = cold water temperature out annulus (°C) = hot water temperatures enter the deep $T_{h,in}$ pipe (°C)

= hot water temperature out the deep pipe $T_{h.out}$

 $\bar{T}_{w,o}$ = average temperature of the outer wall of inner pipe (°C)

= overall heat transfer coefficient based on U_i inner pipe surfaces (W/m².°C)

= overall heat transfer coefficient based on U_{o} the outer surface of the deep pipe $(W/m^2.°C)$

V= average speed of hot water at inner pipe(m/s)

Y = twist ratio

= inner pipe volumetric flow rate of hot Ÿ water (m³/s)

= pumping power (W) \dot{W}_{pump}

= hot water inner pipe density (kg/m³)

= heat transfer increased ratio η

= inner pipe dynamic viscosity of hot water μ (kg/m.s)

= height altitude fluid manometer (m) Δh

= pressure drop (Pa)

 ΔT_{LMTD} = the average logarithmic temperature difference (°C)

REFERENCE

Bergles, A.E., 1985, Techniques to Augment Heat Transfer. In:Rohsenow, W.M., Hartnett, J.P., Ganie, E. (Eds.), Handbook of Heat

- Transfer Application, McGraw-Hill, New York.
- Cengel, Y.A., Cimbala, J.M., 2006, Fluid Mechanics: Fundamental and Applications, 1st edition, McGraw–Hill, New York
- Holman, J.P., 2010, Heat Transfer, 10th ed., McGraw-Hill. New York
- Lavine, A.S., Incropera, F., and De Witt, D., 2006, Fundamentals of Heat and Mass Transfer. John Wiley & Sons; 6th edition (March 10,
- Kreith, F., Manglik, R., and Bohn, M., 2010, Principles of Heat Transfer, Cengage learning.
- Manglik, R.M., and Bergles, A.E., 1992, Heat Transfer Enhancement and Pressure Drop in Viscous Liquid Flows in Isothermal Tubes Twisted-Tape Inserts, Wärme-und Stoffübertragung, Vol. 27 (4), pp. 249-257.
- Murugesan, P., Mayilsamy, K., and Suresh, S., 2010, Turbulent Heat Transfer and Pressure Drop in Tube Fitted with Square-Cut Twisted Tape, Chinese Journal of Chemical Engineering, Vol. 18 (4), pp. 609-617.
- Murugesan, P., Mayilsamy, K., and Suresh, S., 2011a, Heat Transfer and Friction Factor in a Tube Equipped with U-Cut Twisted Tape Insert, Jordan Journal of Mechanical and Industrial Engineering, Vol. 5 pp. 559-565.
- Murugesan, P., Mayilsamy, K., Suresh, S., and Srinivasan, P., 2009, Heat Transfer and Pressure Drop Characteristics of Turbulent Flow in a Tube Fitted with Trapezoidal-Cut Twisted Tape Insert, International journal of academic research, Vol. 1 (1).
- Pratik P. Ganorkar, R.M. Warkhedkar, 2015, Heat Transfer Enhancement in a Tube Using Elliptical-Cut Twisted Tape Inserts, International journal of mechanical engineering, Vol 2.
- Quazi, I., and Mohite, V. 2015, Heat Transfer Enhancement in a Heat Exchanger Using Punched and V-Cut Twisted Tape Inserts.
- Suresh, K.P., Raju, K., Mahanta, P., and Dewan, A., 2005, Review of Passive Heat Transfer Augmentation Techniques, Proceedings of the Institution of Mechanical Engineers (I-Mech-E) Part A, Journal of Power and Energy, Vol. 218 (7), pp. 509-527.
- Petukhov, B., 1970, Heat Transfer and Friction in Turbulent Pipe Flow with Variable Physical Properties, Advances in heat transfer, Vol. 6 (503), pp. i565.
- Salam, B., Biswas, S., Saha, S., and Bhuiya, M.M.K., 2013, Heat Transfer Enhancement in a Tube Using Rectangular-Cut Twisted Tape Insert, Procedia Engineering, Vol. 56 pp. 96-103.

- White, F.M., 2003, *Fluid Mechanics*, (2003). McGraw-Hill.
- Yunus, A.C., 2003, Heat Transfer: A Practical Approach, MacGraw Hill, New York, Vol.

EXPERIMENTAL STUDY THE EFFECT OF SLANT ANGLE ON THE IMPROVEMENT OF HEAT TRANSFER IN COPPER PIPE CONCENTRIC EXPORTER WITH LOUVERED STRIP INSERT FORWARD STRUCTURE

Indra Setyawan ¹, Agung Tri Wijayanta², Tri Istanto ²

¹Student, ²Lecturer– Mechanical Engineering Department–Universitas Sebelas Maret

Keywords:

Friction factor Louvered strip insert friction factor Nusselt number Slant Angle

Abstract:

This study was conducted to investigate the effect of slant angle (α) on heat transfer enhancement in concentric pipe heat exchanger with forward arrangement of louvered strip insert. In this study, louvered strip insert is varied with $\alpha = 15^{\circ}$, 20° and 25° . For comparison, in this study also tested the heat exchanger without insert (plain tube). The working fluid in the inner tube was hot water and in the annulus was cold water, with the flows direction were counterflow. Tests were conducted at a Reynolds number (Re) 5300 -17,500. The study result show that an increase in the Nusselt number (Nu), friction factor (f), and heat transfer enhancement. Characteristics of Nusselt number (Nu) friction factor (f), and heat transfer enhancement ratio with the addition of louvered strip insert increases with increasing slant angle (α). At 5300 < Re < 17500 the value of Nui in the inner pipe with the addition of louvered strip insert with $\alpha = 15^{\circ}$, 20° and 25° increases in the range of 19.04% - 22.86%, 48.09% - 54.83%, and 67.43% - 77.02% compared with Nui of plain tube respectively. At Re 5300 < Re < 17500 The value of friction factor in the inner pipe with the addition of louvered strip insert with $\alpha = 15^{\circ}$, 20° and 25° is 1.52, 2.56 and 3.35 times greater than friction factor of plain tube respectively. Heat transfer enhancement ratio with addition of louvered strip insert with $\alpha = 15^{\circ}$, 20° and 25° in the range of 1.00 - 1.06, 1.02 - 1.08and 1.03 - 1.12 respectively.

1. INTRODUCTION

The heat exchanger is well-known to be used in industry and engineering applications. Its design procedure is complex, as it requires precise analysis of heat transfer rates, efficiency and pressure reduction, regardless of issues such as the long-term performance and economic aspects of the apparatus. To diminish its dimension, cost, and energy saving, a numerous techniques have been purposed to improve its rate from the walls. In every insert technology utilization is applied to intensify the heat transfer, pressure drop also roses up, which affects the pumping costs highy increased. Therefore. enhancements or methods which were used should be optimized between the advantages of heat transfer coefficients escalation and pumping costs due to the friction losses enchancement.

The heat transfer enhancement methods can be broadly classified into three types: passive techniques, active techniques, and mixed techniques. Techniques that do not require additional resources are called passive techniques as examples: turbulence, surface coating, underlying surfaces, surface variations, etc. On the other hand, the active techniques expect additional resources such as mechanical aid, fluid surface vibration, injection, fluid suction, and the electrostatic field applications, which are relatively lack attention in its research and

practice, as they demand higher costs than passive techniques.

Pipe insertion passive technique provides several advantages over other heat transfer techniques, such as can be applied to the smooth pipe contained in heat exchanger and the inserts can maintain the fine pipe mechanical strength. The installation is easy, the cost is cheap, and relatively convenient to take for cleaning process. It includes louvered strip insertion, delta winglet, perforated twisted tape, etc. The heat transfer enchancement of turbulent elements utilization become the one of these applications to improve the flow surface heat transfer coefficient through the turbulent movement escalation. The common mechanism of gaining the heat transfer by using pipe inserts is turbulator able to boost turbulence and also can reduce thethe thermal boundary layer thickness.

2. RESEARCH METHODS

Hot water fluid flows in the inner tube on the closed trajectory. It comes from a hot water tank which is pumped into a pipe in a heat exchanger, then going out, and back again into. The heater was utilized to boil water on water tank at steady temperature of 60°C. The testing apparatus schematic can be seen in Fig. 1. The fluid flow direction in the inner pipe and the annulus were counterclockwise.

Cold water was pumped into the cold water tank at the top. The water level height in the tank was kept constant which caused the cold water flowing flowed into the annulus to keep constant by utilizing the gravity. The cold water which spilled in the annulus was an open path, so it is immediately discharged into the environment. The entry temperature into the annulus was maintained $\pm 28^{\circ}$ C.

A U-shaped manometer was utilized to measure a pressure differences in hot water which circulating on the inlet and outlet side. A water fluid was used in the manometer. Water trap was used to hold the carried water during the measuring process of the manometer pressure due to block to enter the manometer.

Heat exchanger, one-way concentric pipe with inner and outer pipe were made of aluminum. Its dimensions can be seen in figure 2. Type-K thermocouple was used to measure hot water temperature in and out of inner pipe, outer wall of deep pipe, and cold water enter and exit annulus. The outer wall temperature measurement of the inner pipe was 10 points, as shown in FIG. 2 which symbolized by Tw.

A study of the effect of louvered strip insert angle on heat transfer characteristics and friction factor on concentric heat exchangers, it were varied by 15° , 20° , and 25° of angle of attack (α) with 40 mm of gap of pitch inserts, a louvered strip insert mounting scheme can be seen in figure 3.

Reynolds number of water flow in inner pipe were varied by adjusting 2-6 LPM of flow rate for inner pipe without louvered strip insert (plain tube) and inner pipe with additional louvered strip insert. The collected data was the data

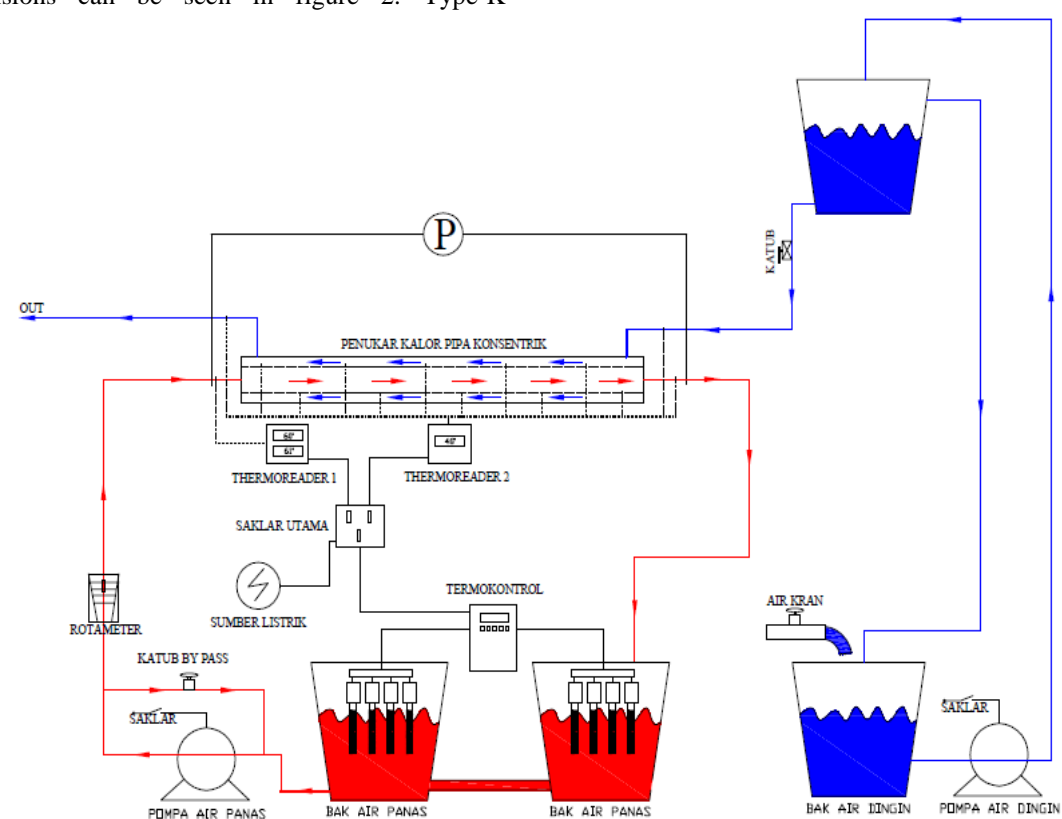


Figure 1. Scheme of concentric pipe heat exchanger testing using louvered strip insert.

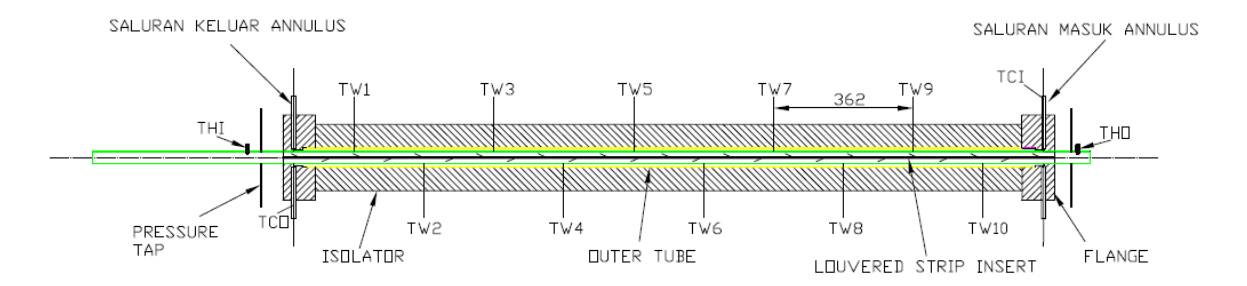


Figure 2. Scheme of concentric pipe heat exchanger for louvered strip insert.

obtained by the inlet and outlet temperature of the inner pipe, the inlet and outlet exit water temperature, the outer wall temperature of the inner pipe, the mass water flow rate in the inner pipe and annulus, and the pressure drop in the inner pipe. For each test variations, datas were taken every 10 minutes until steady state has been obtained. It utilized in the research data calculation and analysis. For comparison, tests were also conducted on inner tubes without louvered strip inserts and with the louvered strip inserts addition, Nusselt results and

friction factors were also incorporated by Eimsa Ard, 2008 for validation.

Heat Transfer Characteristics Calculation, Friction Factor, and Heat Transfer Ratios of Concentric Pipes Heat Exchanger

Heat transfer rate in the inner pipe can be expressed as:

$$Q_{h} = m.C_{p.h}.(T_{h.i} - T_{h.o}) = U_{i}A_{i}\Delta T_{LMTD}$$
 (1)

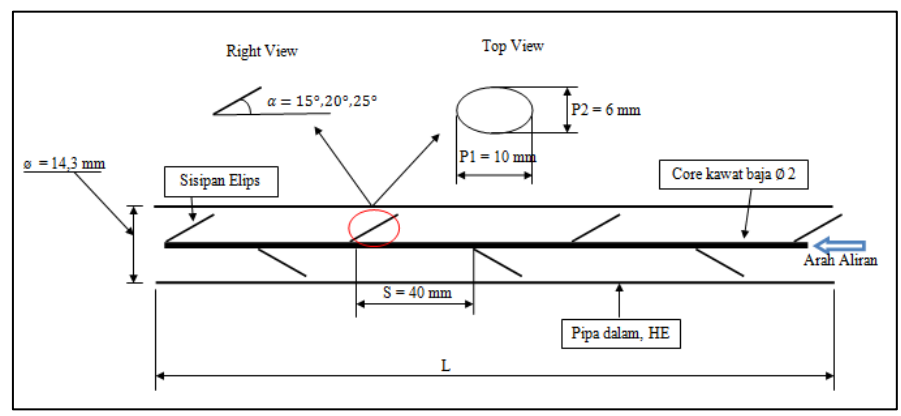


Figure 3. Scheme of louvered strip insert mounting in the inner pipe



Figure 4. Louvered insert strips which used in the study

Heat transfer rate to cold water on the annulus side can be calculated by:

$$Q_{c} = m.C_{p,c}.(T_{c,o} - T_{c,i}) = h_{o}.A_{o}.(\overline{T}_{w,o} - T_{b,c})$$
(2) where

$$T_{b,c} = \frac{T_{c,i} + T_{c,o}}{2} \operatorname{dan} \overline{T}_{w,o} = \frac{\sum_{i=1}^{i=10} T_{w,i}}{10}$$
(3)

Heat loss Percentage ((Q_{loss})) can be calculated by:

$$\% \ Q_{loss} = \left[\frac{Q_h - Q_c}{Q_c} \right] \times 100\%$$
 (4)

The overall heat transfer coefficient based on the inner pipe surface area can be calculated using equation (5):

$$U_i = \frac{Q_h}{A_i \, \Delta T_{LMTD}} \tag{5}$$

where, the value ΔT_{LMTD} of counterflow heat exchangers can be formulated with:

$$\Delta T_{LMTD} = \frac{\Delta T_2 - \Delta T_1}{\ln\left(\Delta T_2/\Delta T_1\right)} = \frac{\Delta T_1 - \Delta T_2}{\ln\left(\Delta T_1/\Delta T_2\right)}$$
(6)

where, $\Delta T_l = (T_{h.i} - T_{c,o})$ dan $\Delta T_2 = (T_{h.o} - T_{c,i})$. The mean value of convection heat transfer coefficient on the annulus side can be calculated by:

$$h_o = \frac{Q_c}{A_o \left(\overline{T}_{w,o} - T_{b,c} \right)} \tag{7}$$

The mean value of convection heat transfer coefficient on the inner pipe side can be calculated as follows:

$$\frac{1}{U_i A_i} = R_{total} \tag{8}$$

$$\frac{1}{U_{i}.A_{1}} = \frac{1}{h_{i}.A_{i}} + \frac{\ln(d_{o}/d_{i})}{2\pi k_{p}L} + \frac{1}{h_{o}.A_{o}}$$
(9)

where

$$A_i = \pi.d_i$$
. L
 $A_o = \pi.d_o$. L

thus, the convection heat transfer coefficient on the inner pipe side is as follows:

$$h_{i} = \frac{1}{\left[\frac{1}{U_{i}} - \frac{d_{i} \cdot \ln(d_{o}/d_{i})}{2k_{p}} - \frac{d_{i}}{d_{o} \cdot h_{o}}\right]}$$
(10)

The mean value of Nusselt number in the inner pipe can be calculated by:

$$Nu_i = \frac{h_i . d_i}{k_{fi}} \tag{11}$$

The heat exchangers effect can be calculated by:

$$\varepsilon = \frac{Q_{aktual}}{Q_{maksimum}} = \frac{Q_h}{C_{\min}.(T_{h,i} - T_{c,i})}$$
(12)

Pressure drop (pressure drop) in the inner pipe can be calculated with:

$$\Delta P = \rho_{\rm m} \cdot g \cdot \Delta h \tag{13}$$

Pumping power can be calculated with:

$$W_{\text{pompa}} = \overset{\bullet}{V} \cdot \Delta P \tag{14}$$

The friction factor in the inner pipe can be calculated by:

$$f = \frac{\Delta P}{\left(\frac{L_i}{d_i}\right)\left(\frac{\rho \cdot V^2}{2}\right)} \tag{15}$$

Reynolds number of hot water flow in the inner pipe can be calculated with:

$$Re = \frac{\rho . V. d_i}{\mu} \tag{16}$$

where, the hot water properties in the inner pipe $(\rho,$ $k_{\rm fi}$, dan μ) were evaluated at hot bulk water temperature average $(T_{b,h})$.

The heat transfer enchancement ratio on the constant pumping power was the ratio of the average convection heat transfer coefficient of the inner tube insert addition using a plain tube which can be written as follows:

$$HEratio \frac{h_s}{h_p} \bigg|_{pp}$$
 (17)

The characteristics of heat transfer, friction factor, and heat transfer enchancement ratio can be respectively expressed with graph of the relationship between Nu to Re, f to Re, and heat transfer Re. enchancement ratio to Heat

characteristics validation on the inner tube without plain tube is using Petukhov and Gnielinski equations:

Petukhov's equation:

$$Nu = \frac{(f/8). Re. Pr}{1,07+12,7. (f/8)^{1/2}. (Pr^{2/3}-1)}$$
 (18)

The Petukhov equation (18) applies to a fully developed region and applies to $0.5 \le Pr \le 2000$ and $10^4 < \text{Re} < 5 \times 10^6$.

Gnielinski's equation:

$$Nu = \frac{(f/8) \cdot (Re-1000) \cdot Pr}{1 + 12,7 \cdot (f/8)^{1/2} \cdot (Pr^{2/3} - 1)}$$
(19)

The Gnielinski equation (19) applies to fully developed regions and applies to $0.5 \le Pr \le 2000$ and $3 \times 10^3 < \text{Re} < 5 \times 10^6$. Equations (18) and (19) the friction factor value (f) is expressed as follows:

$$f = (0.790 \ln \text{Re} - 1.64)^{-2}$$
 (20)

The pipe heat transfer characteristics validation is using a plain Blasius's equation:

Blasius's equation:

$$f = 0.3164.\text{Re}^{-0.25} \tag{21}$$

 $f = 0.3164 \cdot \text{Re}^{-0.25}$ (21) Equation Blasius (21) applies to $4 \times 10^3 < \text{Re} < 10^5$.

3. RESULTS AND DISCUSSION

a. Plain Tube Validation

Heat transfer characteristics validation has been performed for plain tube using Petukhov empirical correlation and Gnielinski in this research, and also friction factor characteristic validation for plain tube using empirical empiric correlation.

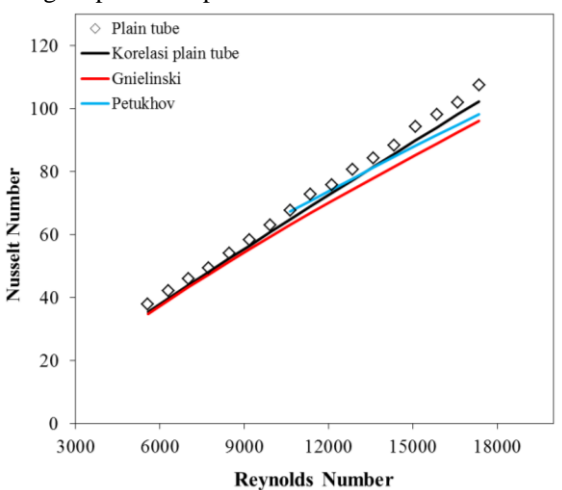


Figure 5. Graph of Nui's relationship using Re for plain tube

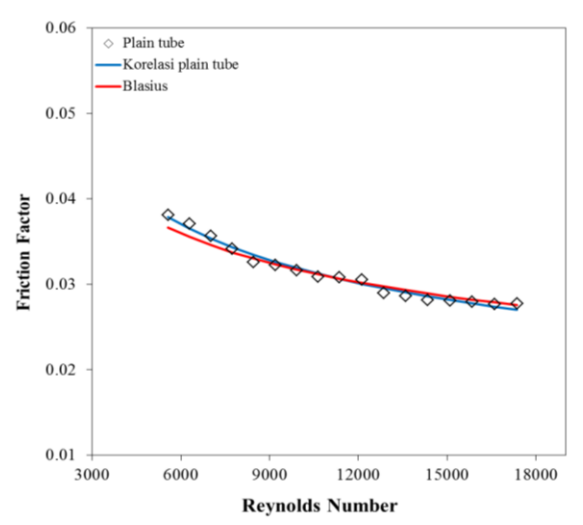


Figure 6. Graph of f relationship using Re for plain tube

Figure 5-6 shows the ratio between Nui and f of the plain tube compared to the the empirical correlation results. Nusselt plain tube number deviations on empirical correlation of Petukhov and Gnielinski were respectively less than $\pm 7.9\%$ and $\pm 4.75\%$. However, plain tube friction factor deviationed to Blasisus correlation was equal $\pm 1.67\%$.

b. The Effect on Angle of Attack to Heat Transfer Characteristics Using Louvered Strip Insert Addition

The inner pipe heat transfer characteristics of concentric pipe heat exchanger can be seen in figure 7.

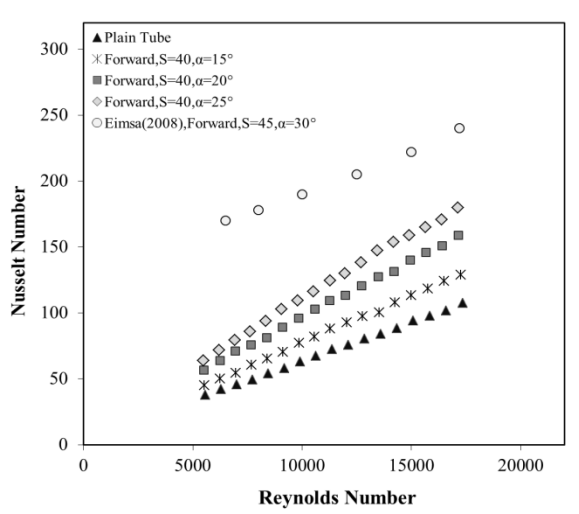


Figure 7. Graph of Nui's relationship to Re

Figure 7 shows that the average Nusselt number (Nui) is increased as long as Reynolds number. It occured for both plain tubes and deep pipes using louvered strip inserts addition. The Nusselt number also climbed as long as the slant angle enchancement and has the maximum value at the slope angle of 25°, it were convenient to Pethkool (2006), Eiamsa-ard (2008) and Mohammed (2013) research. The louvered strip insert addition in the inner pipe can make the Nusselt number increased when compared

to the plain tube. It was caused by the louvered strip insert generated strong turbulence intensity, setting a rapid fluid mixing especially at higher slope angle and disrupting the thermal boundary layer growth (Eiamsa-ard, 2008).

c. The Effect on Angle of Attack to Friction Factor Characteristic of Heat Exchanger Using Added Louvered Strip Insert

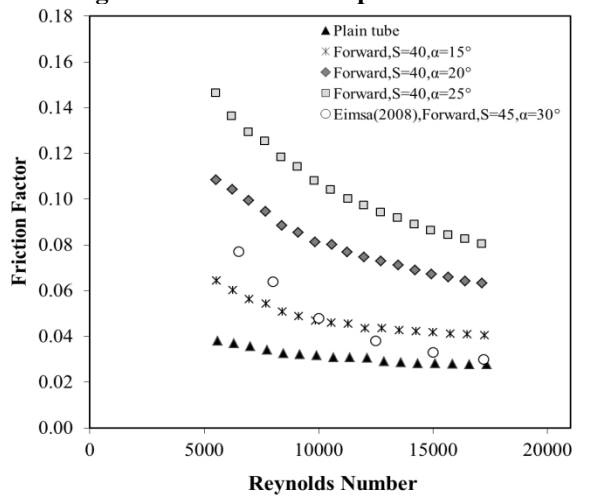


Figure 8. Graph of friction factor relationship to Re

Figure 8 it can be clearly seen that the friction factor value (f) of the pipe is reduced by the Reynolds (Re) number enchancement. The inner pipe friction factor using the louvered strip insert addition was greater than on the plain tube. The friction factor increased as long as the angle of inclination (α) climbed up, it was caused by the greater value of α , the flow resistance was getting bigger. At 5300< Re <17.500 the average friction factor value in the inner pipe using the louvered strip insert addition of $\alpha = 15^{\circ}$, 20° , and 25° were successively 1.52; 2.56; dan 3.35 times greater than plain tube friction factor. The mean value of the inner pipe friction factor using louvered strip insert addition of $\alpha = 25^{\circ}$ were respectively 2.20 and 1.31 times larger than the inner pipe friction factor using the louvered strip insert addition of $\alpha = 15^{\circ}$ and 20° .

From Figure 8 were also compared the results of research to experiments which conducted by Eimsa (2008), at 6200 <Re<17.500 were obtained fraction factor values within 0.028 - 0.077, it can be clearly seen that the research results which conducted by Eimsa at an angle $\alpha = 30^{\circ}$ noticed lower than current research (α =15°, 20°, dan 25°), it caused by larger pipe diameter and pitch distance between inserts has a longer distance of S = 45 mm compared to the distance between pitches in the current study that is S = 40 mm, it produced the pressure difference value which observed Eimsa has a lower value while the friction factor value was directly proportional to the pressure difference value in the inner pipe. It indicates that the distance between the pitch and the cross-sectional area of the pipe affects the friction factor value, the smaller the pitch distance between the inserts and the cross-sectional area of the inner pipe, the higher the friction factor value.

d. The effect on Angle of Attack on Characteristic of Effect of heat exchanger with addition of Louvered Strip Insert

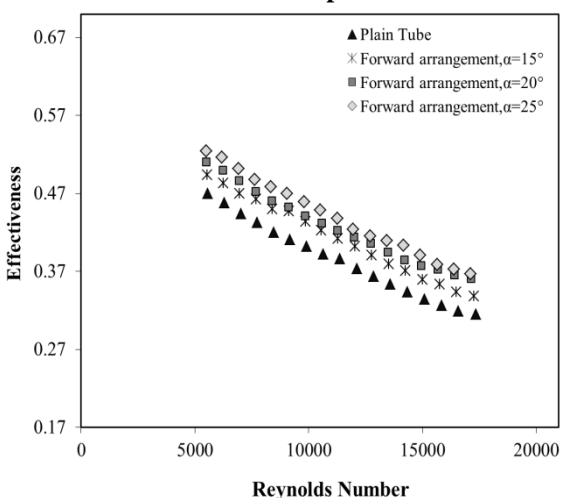


Figure 9. Graph of effectiveness and Re

The effectiveness of a heat exchanger is an actual heat transfer rate ratio that occurs with the maximum possible heat transfer rate. From Figure 9 it can be seen that the effectiveness of heat exchanger decreases with the increase of Reynolds number (Re). The effectiveness of heat exchangers with louvered strip insert inserts is higher than the effectiveness of heat exchangers without insertion (plain tube). From Figure 9 it is seen that the effectiveness of heat exchanger increases with increasing angle of inclination (α) .

From Figure 9 it is found that in the range of 5300 < Re < 17.500, the value of effectiveness of heat exchanger by the addition of louvered strip insert with $\alpha = 15^{\circ}$, 20° dan 25° successively increasing in the range 5.2% - 8.8%; 8.7% - 14.5%; dan 11.6.% - 17.5% compared with plain tube. The value of effectiveness of heat exchanger by the addition of louvered strip insert with $\alpha = 25^{\circ}$ successively increasing in the range 5.0% - 8.8%; and 1.6% - 4.9% compared to the addition of louvered insert strips with $\alpha = 15^{\circ}$ dan $\alpha = 20^{\circ}$.

e. The Effect on Angle of Attack to Heat Transfer Ratios Louvered Strip Insert Ratio

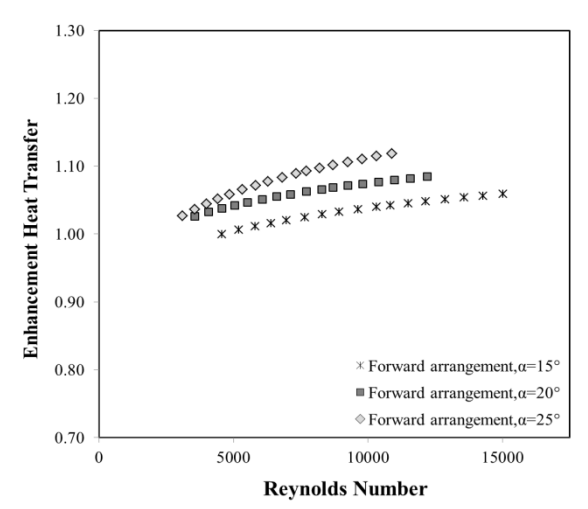


Figure 10. Graph of relation ratio increase to heat transfer with Re

From Figure 10 it can be seen that at 3000 <Re <15,500 the ratio of increase of heat transfer from heat exchangers to louvered strip insert inserts increases with the increase of Reynolds number. The increase of heat transfer ratio also increases with the increment of slope angle (tor). This was consistent with Fan (2012) research, in the fan research which can bee seen that the Reynolds number 10,000 -17,500 the increased heat transfer ratio value increased, then with Reynolds number above 17,500 - 42.500 the heat transfer ratio value decreases, this was because of high Reynolds number inflows into the pipe in high speed moving then meet with the strong turbulence that was happening in the deep pipe and collide with each other causing the effect of turbulence in the pipeline in the down and the boundary layer becomes thicker which followed by the decrease value of heat transfer.

Increased heat transfer ratio of heat exchanger by addition of inserted louvered strip insert at $\alpha=15^\circ, 20^\circ$ dan 25° successively in the range 1.00 - 1.06; 1.02 - 1.08; and 1.03 - 1.12. This means that at the same pumping power, the average convection heat transfer coefficient value in the inner pipe with the addition of louvered strip insert was greater than the value of the average convection heat transfer coefficient of plain tube.

4. CONCLUSION

Nusselt number and friction factor of heat exchanger by addition of louvered strip insert was increased with increasing angle of attack (α). Heat exchanger with the louvered strip insert addition with 25° on angle of attack produced highest Nusselt number, pressure drop, friction factor, effektivenes, and heat transfer rate.

NOTASI

 A_i = surface area inner pipe (m²)

 A_o = external surface area of inner pipe (m²) $A_{t,i}$ = the inner pipe cross-sectional area (m²)

- $A_{t,S}$ = the inner pipe cross-sectional area with the insertion (m²)
- $C_{p,c}$ = spesific heat cold water (kJ/kg. $^{\circ}$ C) $C_{p,h}$ = spesific heat hot water (kJ/kg. $^{\circ}$ C)
- $D_{h,i}$ = inner pipe hydraulic diameter $D_{h,o}$ = anulus hydraulic diameter
- f = friction factor
- h_i = convection heat transfer coefficient inner pipe mean (W/m².°C)
- h_o = convection heat transfer coefficient mean *annulus* (W/m².°C)
- h_p = convection heat transfer coefficient mean value at inner pipe louvered strip insert (W/m².°C)
- h_s = convection heat transfer coefficient mean value at inner pipe louvered strip insert (W/m².°C)
- k_i = mean of hot water thermal conductivity inner pipe (W/m. $^{\circ}$ C)
- L_t = pressure drop measurement length At inner pipe (m)
- \dot{m}_c = cold water mass flow rate (kg/s)
- \dot{m}_h = mass flow rate of hot water (kg/s)
- $\begin{array}{ll} Nu_i & = mean \ value \ of \ Nusselt \ number \ at \ inner \\ pipe & \end{array}$
- Nu_o = mean value of Nusselt number at annulus
- pp = equal pumping power
- Q_c = the annulus heat transfer rate (W)
- Q_h = the inner pipe heat transfer rate (W)
- Q_{loss} = convection at inner pipe heat loss (W)
- Re = Reynolds Number
- $T_{b,o}$ = mean value of bulk temperature at annulus (${}^{\circ}C$)
- $T_{c,in}$ = cold water temperature enter the annulus (${}^{o}C$)
- $T_{c,out}$ = cold water temperature out annulus (${}^{\circ}C$)
- $T_{h,in}$ = hot water temperatures enter the inner pipe (${}^{\circ}C$)
- $T_{h,out}$ = hot water temperature out the inner pipe (${}^{\circ}C$)
- $\overline{T}_{w,o}$ = mean temperature of the outer wall of the pipe dalam (°C)
- U_i = overall heat transfer coefficient based on inner pipe surfaces (W/m².°C)
- U_o = overall heat transfer coefficient based on the outer surface of inner pipe (W/m².°C)
- V = hot water average speedof inner pipes(m/s)
- \dot{W}_{pump} = pumping power (W)
- ρ = hot water of inner pipe density (kg/m³)
- μ = hot water dynamic viscosity of inner pipe (kg/m.s)
- α = angle of attack (°)
- ΔP = pressure drop (Pa)
- ΔT_{LMTD} = mean value of logarithmic temperature difference ($^{\circ}$ C)

REFERENCE

- Anindito, 2013, Pengaruh *Double-Sided Delta Wing Tape Insert With Alternate-Axis* Terhadap
 Karakteristik Perpindahan Panas dan Faktor
 Gesekan pada Penukar Kalor Pipa
 Konsentrik, UNS, Surakarta, Indonesia.
- Arifad, 2014, Pengaruh Wing Pitch Ratio dan Wing Width Ratio Terhadap Karakteristik Perpindahan Panas Dan Faktor Gesekan Pada Penukar Kalor Kalor Pipa Konsentrik dengan Double Sided Delta Wing Tape Insert Susunan Forward Wing, UNS, Surakarta, Indonesia.
- Cengel, Y.A., 2003, *Heat Transfer: A Practical Approach*, 2nd edition, McGraw–Hill, New York
- Cengel, Y.A., Cimbala, J.M., 2006, Fluid Mechanics: Fundamental and Applications, 1st edition, McGraw-Hill, New York
- Eiamsa-ard, S., Pethkool, S., Thianpong, C., Promvonge, P., 2008, Turbulent flow heat transfer and pressure loss in a double pipe heat exchanger with louvered strip inserts, *International Communications in Heat and Mass Transfer*, Vol. 35, pp. 120–129
- Fan, A.W., Deng, J.J., Nakayama, A., Liu, W., 2012, Parametric study on turbulent heat transfer and flow characteristicsin a circular tube fitted with louvered strip inserts, *International Journal of Heat and Mass Transfer*, Vol. 55, pp. 5205–5213
- Incropera, F.P., DeWitt, D.P., 2006, Fundamentals of Heat and Mass Transfer, 6th Ed, John Willey and Sons, New York.
- Mohammed, H.A., Hasan, H.A., Wahid, M.A., 2013, Heat transfer enhancement of nanofluids in a double pipe heat exchanger with louvered strip inserts, *International Communications in Heat and Mass Transfer*, Vol. 40, pp. 36–46
- Pethkool, S., Eiamsa-ard, S., Ridluan, A., and Promvonge, P., 2006, Effect of louvered strips on heat transfer in a concentric pipe heat exchanger, *The 2nd Joint International Conference on "Sustainable Energy and Environment (SEE 2006)"*, 21-23 November 2006, Bangkok, Thailand
- Pranata Adi, 2013, Pengujian Karakteristik Perpindahan Panas dan Faktor Gesekan Pada Penukar Kalor Pipa Konsentrik Dengan *Double-Sided Delta-Winglet Tape Insert*, UNS, Surakarta, Indonesia.

TWO-PHASE FLOW CHARACTERISTICS ON THE EXTENSIVE EXPANSION CHANNEL

Latif Ngudi Wibawanto¹, Budi Santoso², Wibawa Endra Juwana²

¹Student, ²Lecturer– Mechanical Engineering Department–Universitas Sebelas Maret

Keywords:

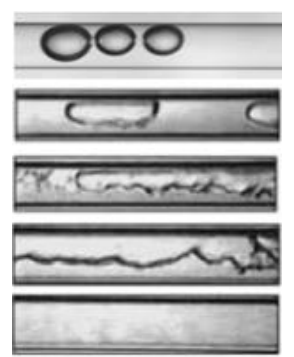
Two phase flow Flow current Expansion Pressure recovery

Abstract:

This research was conducted to find out the flow characteristic of two phases through channel with sudden expansion in the form of change of flow pattern and pressure recovery. The test was conducted with variation of superficial velocity of water 0.2-1.3~m / s and superficial air velocity of 0.2-1.9~m / s resulting in pattern of three flow patterns ie bubble, plug, and slug. The expansion channel resulted in some changes to the flow pattern that originally plugs in the upstream channel into bubble in the downstream channel and the slug becomes plug. Pressure recovery experimental results were compared with the homogeneous model flow equation and Wadle correlation, the two correlations had predictions with standard deviation values of 0.32~and~0.43.

INTRODUCTION

The two-phase flow is part of a multi-phase flow. The flow of these different phases is commonly used in industrial processes, energy conversion system components such as heat exchangers, evaporators, and cooling cycles. These components are commonly applied components in industrial processes and nuclear power installations. The petroleum products transport which concerns in pipes has been become a number of studies object that construct design models of flow/ pattern type and pressure drops in vertical, horizontal, and tilted pipes. The particular flow pattern in Figure 1 is formed due to the velocity combination of the liquid and gas phases that depending on the pipe gravitational interaction, inertia, and surface tension. It is believed that the squared flow mechanisms and a small diameter of circular cross-section (mini channels) differ from channels with larger diameters (conventional channels).



- (a) Bubble
- (b) Plug
- (c) Slug
- (d) Wavy
- (e) Annular

Figure 1. Two-phase flow pattern on the horizontal channel

This flow pattern affects the pressure distribution along the channel, its pressure drop and pressure recovery which have a contraction and expansion. The flow pattern type on heat exchange system influences the heat transfer coefficients.

The transition area of bubble-plug flow pattern can be predicted by recognizing the value of d_b/D_h that lies between 0.03-0.4. It depends on the bubble pattern vacuum fraction value at the area around the transition boundary (α_{cr}) which is obtained from the following equation:

$$\alpha_{cr} = 0.6-2.32 \, \frac{d_b}{D_b}$$
 (1)

$$J_{g} = u_{g} \cdot \alpha \tag{2}$$

The fluid disposition is generally performed by utilizing piping systems in some industries such as chemical industry. It require major pipes, it also need several pipeline components, such as pipe bends, elbows, valves, expansion channel, compression channel, and combinations channel. In large pipeline systems, the pipe components losses are usually a minor (minor loss) loss compared to friction losses along the channel (major losses). However, to the contrary system, the pipe component losses can be a major disadvantage to total losses along the flowing path. Pressure recovery develops quick expansion on channel area, i.e., the greater pressure after the expansion due to the fluid velocity significantly decreased and the pressure will do so. Apparatus designing process become necessarily to estimate the two-phase flow drop characteristics. The pressure recovery value is calculated to determine the piping system total losses. The pressure recovery research of two-phase flow has been accomplished to obtain the technical guidance and practical design in components procedure of energy conversion system as in the pump specifications selection which is used on the system. In this experiment, it will be carried out by using a mini-sized square-sectional test channel on conventional upstream and rectangular channels in the downstream channel utilizing air and water as the working fluid. The pressure recovery value ΔP_e , due to the expansion is defined as the pressure difference when the pressure gradient line at the flow conditions developing full upstream and downstream is extrapolated to the channel extension point (P1 and P2) shown in Figure 2. This study is to predict the pressure recovery value using homogeneous flow method (Equation 3) and the Wadle Equation (1988) (Equation 4).

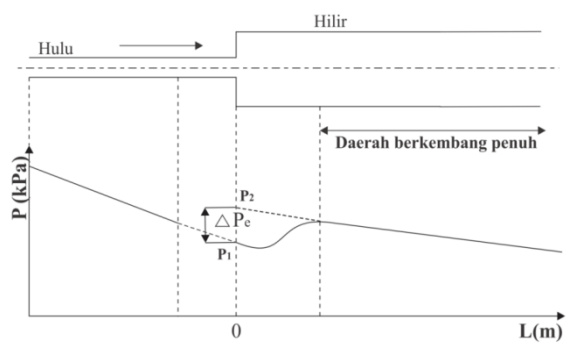


Figure 2. The pressure distribution on the channel of instant expansion.

The pressure recovery value is determined by the following equation:

$$\Delta P_{e} = (1 - \sigma^{2}) \frac{1}{2} G_{\text{total}}^{2} K \left[\frac{x}{\rho_{g}} + \frac{1 - x}{\rho_{l}} \right]$$
 (3)

$$\Delta P_{e} = (1-\sigma^{2}) \frac{1}{2} G_{\text{total}}^{2} K \left[\frac{(1-x)^{2}}{\rho_{1}} + \frac{x^{2}}{\rho_{o}} \right]$$
 (4)

dimana,

X = gas quality

 σ = expansion ratio (A_1/A_2)

A = channel area, m^2

G = mass flux phase, kg/m²s ρ_h = mixture density, kg/m³ ΔP_e = pressure recovery, kPa

K = empiric phase air-water (0.83)

Subscript,

1 = upstream channel 2 = downstream, channel 1 = liquid phase (air) g = gas phase (udara)

RESEARCH METHODOLOGY

The test was performed by using variation of J₁ 0.2-1.3 m/s of superficial water velocity and Jg 0.2-1.9 m/s of superficial air velocity. The test and instrumentation scheme are shown in Fig. 3 and Fig. 4. The two-phase flow pattern in each variation, the camera is placed over the channel that is on the upstream channel to observe its value, expansion area, and downstream with 3 seconds of recording duration. A lamp was placed under the test channel to make the image obtained more clearly, the camera which was used in this study has 1000 fps of shooting speed. The two-phase flow recording video

was processed using Phantom 630 software to determine the gas phase actual speed (u_g) . The pressure measurements were performed on full fledged areas. It was taken at of 0.6-1.3 m/s of water superficial velocity. The test line has five pressure taps as a pressure measuring point on each upstream and downstream channel. The PA500-501G Copal pressure sensor was used to measure the pressure at the first pressure gauge and the MPXV4006DP pressure sensor was used to measure the pressure difference between the first pressure measuring point and the next measuring point.

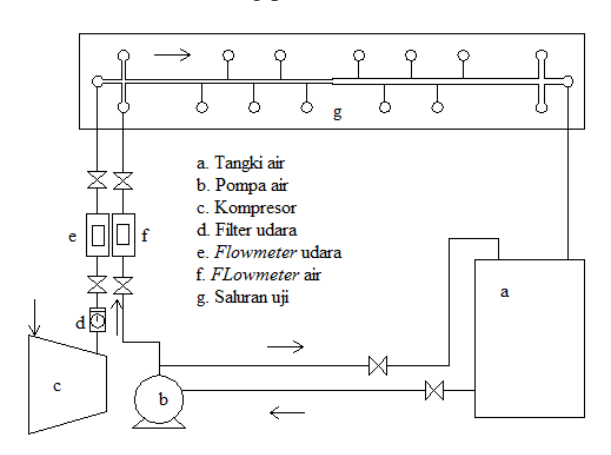


Figure 3. Test scheme

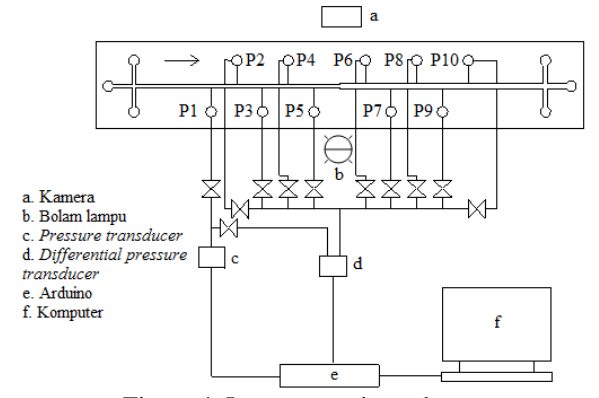


Figure 4. Instrumentation scheme

RESULT AND DISCUSSION

Two-phase flow pattern

The identified results flow patterns of this study are as follows:

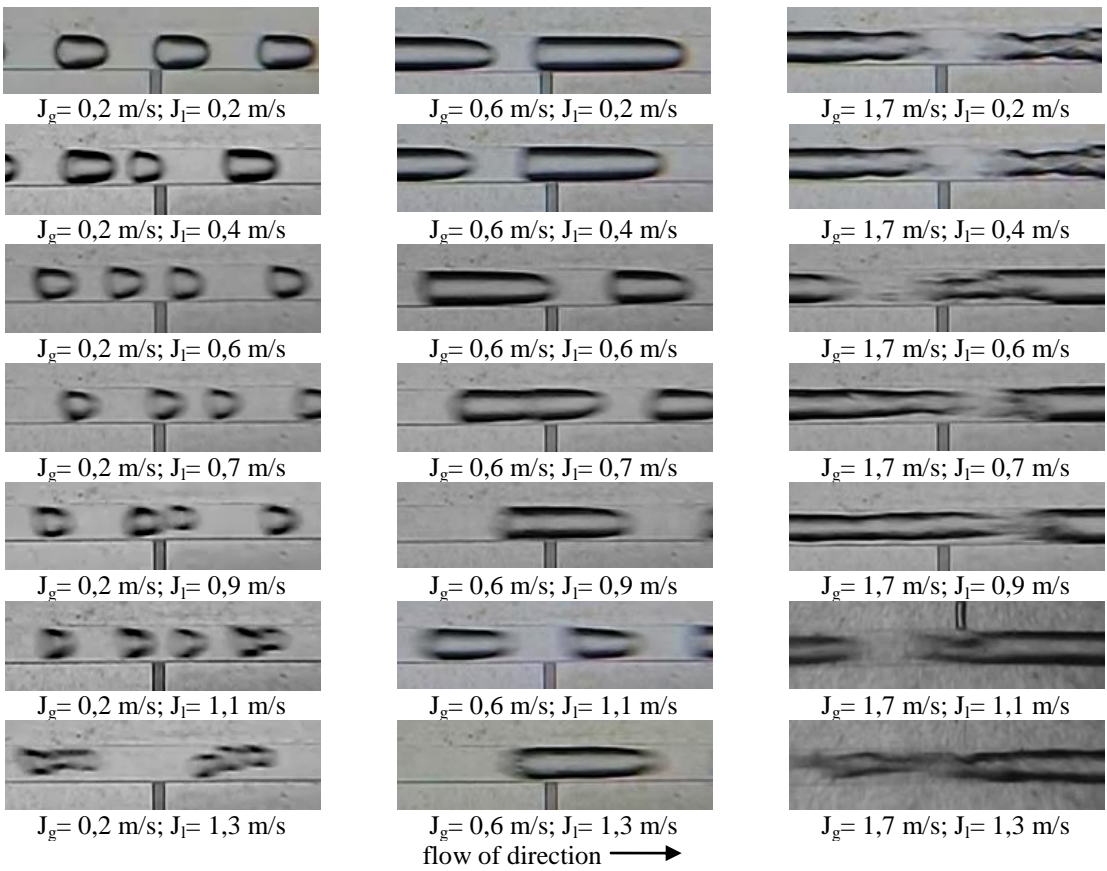


Figure 5. Two-phase flow pattern on the channel

In this research, there were three different flow patterns, namely bubble, plug, and slug, while wavy and annular flow patterns were not found in this study. Figure 5 shows some flow patterns that exist in this study. The bubble flow pattern begins to be found in a water flow variation of 300 ml/min at a superficial velocity of 0.6 m/s, this pattern is formed only at 0.2 m/s and 0.4 m/s of low superficial air velocities. At the superficial velocity variations 0.2 m/s and 0.4 m/s bubble flow patterns were not found even at low superficial air velocities. Bubble becomes more elongated which then turns into a plug along with increasing superficial air velocity at the same superficial water velocity. The slug flow pattern was formed at a superficial high air velocity variation. The slug flow pattern was started to form at 1.7 m/s and 0.2 m/s of superficial velocity.

The flow pattern data visualization of research results on the upstream channel was plotted on the flow pattern map made by Zhao (Figure 6) which equally used mini sized channel yet utilizing different channel hydraulic diameter.

Based on the experimental data and flow pattern map, there was a slight difference (shift) of the transition region between the bubble and the plug. This difference can be due to the diameter of the hydraulic channel which was used in this study three times greater than the channel used by Zhao.

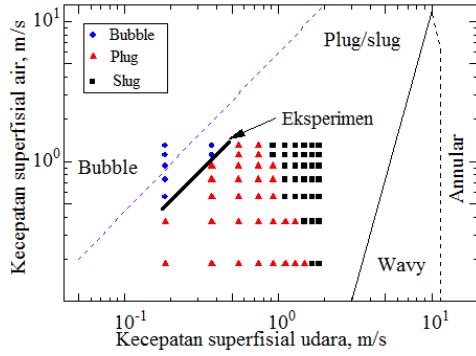


Figure 6. The research results flow pattern was plotted on the flow pattern map Zhao (2004)

The transition region of the bubble-plug flow pattern can be predicted by knowing the value d_b/D_b between 0.03-0.4 shown in Table 1.

Table 1. Dimensionless parameter data d_b/ at bubble-plug transition region

J _l , m/s	J_g ,	$u_{g,}$	$\alpha_{\rm cr}$	pola aliran	d _b /D _h
	m/s	m/s			
0,6	0,2	1,4	0,13	Bubble	0,20
0,7	0,2	1,6	0,11	Bubble	0,21
0,9	0,2	2,1	0,09	Bubble	0,22
1,1	0,4	2,4	0,16	Bubble	0,19
1,3	0,4	2,7	0,14	Bubble	0,20

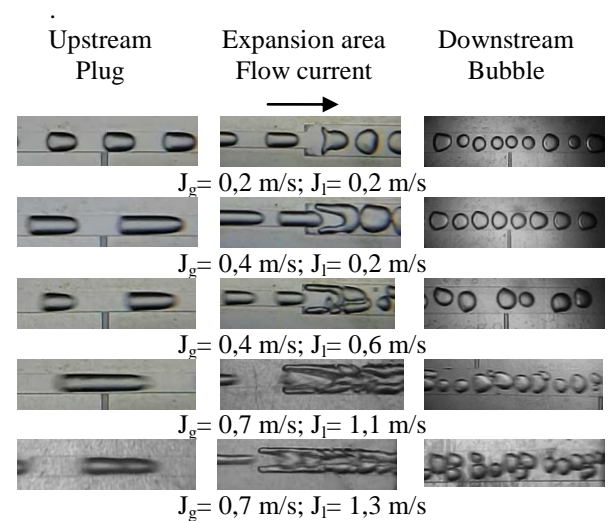


Figure 7. Plug flow pattern transformation to bubble

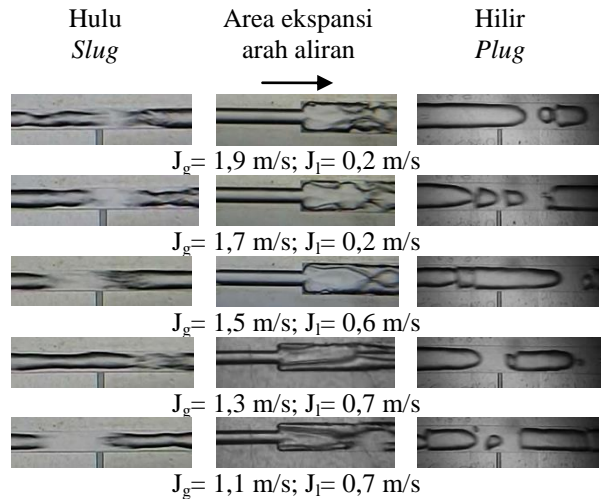


Figure 8. Slug flow pattern transformation to plug

Channel expansion results in some flow patterns transformation to different pattern types was performed by this research. Such as, $J_l=0.2$ m/s, $J_g=0.4$ m/s dan $J_l=0.6$ m/s, $J_g=0.4$ m/s of flow patterns that were originally plug turned into bubble as shown in Figure 7. The bubble flow pattern on the downstream channel was more common than before the flow passes through the expansion (in the upstream channel). At $J_l=0.2$ m/s, $J_g=1.9$ m/s dan $J_l=0.7$ m/s; $J_g=1.1$ m/s the flow pattern originally slugs

into a plug is shown in Figure 8. The plug flow pattern on the downstream channel was less than before the flow goes through the expansion

2. Pressure recovery

The transition region length (L_d) at the instant expansion channel which shown at Table 2 is a function of the Reynolds number on the upstream channel (Re₁). The transition region length gets bigger as the Reynolds number increases. The comparison value between the transition region length and the channel diameter (L_d/D_h) on the expansion channel can be correlated based on Reynolds number and expansion ratio (σ). In this study, pressure measurements were taken at a distance of 30 mm after expansion. The Reynolds number used was the total Reynolds number of each phase. Based on Equation 5, the distance was already in full developing region therefore in Figure 9 the pressure distribution before in the transition region was unknown.

$$\frac{L_d}{D_h} = 13,788. \text{ Re}_1^{0,11} (1-\sigma)^{2,463}$$
 (5)

The pressure recovery value $\Delta P_{\rm e}$, since the expansion was defined as the pressure difference when the pressure gradient line at the flow condition was fully developed upstream and downstream was extrapolated to zero on the extension channel. Figure 10 shows that the greater the superficial velocity of water, the greater the pressure recovery value. At the same superficial water velocity the larger quality of the pressure recovery gas quality value also tends to be bigger. From the figure 9 can be seen that the value of pressure recovery research results were closer to the recovery pressure value obtained from the homogeneous flow model equation than the correlation Wadle (1988).

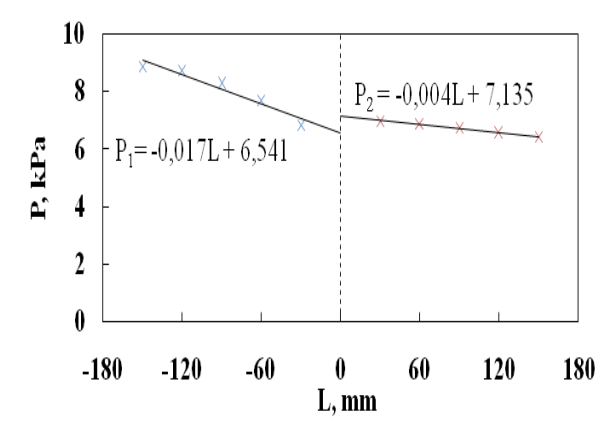


Figure 9. Pressure distribution along the channel of instant expansion of J_l = 0,9 m/s, J_g = 0,6 m/s

Table 2. The expansion channel length at ransition region

region.	ı	1	ı	ı
	J _g , m/s	Re udara	Re total	L _d , mm
J _l , m/s	0,7	139,2	2220,1	23,2
0,6	0,9	174,0	2254,9	23,2
Re air	1,1	208,8	2289,7	23,3
2080, 9	1,7	313,2	2394,1	23,4
J _l , m/s	0,6	104,4	3572,5	24,4
0,9	0,7	139,2	3607,3	24,4
Re air 3468,	0,9	174,0	3642,1	24,5
1	1,1	208,8	3676,9	24,5
	1,7	313,2	3781,3	24,6
J _l , m/s	0,2	34,8	5583,8	25,6
1,3	0,4	69,6	5618,6	25,7
	0,6	104,4	5653,4	25,7
Re air 5549,	0,7	139,2	5688,2	25,7
0	0,9	174,0	5723,0	25,7
	1,1	208,8	5757,8	25,7
	1,5	313,2	5792,6	25,8

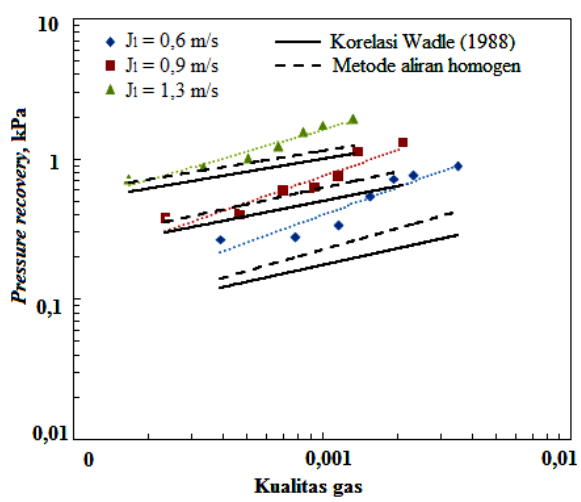
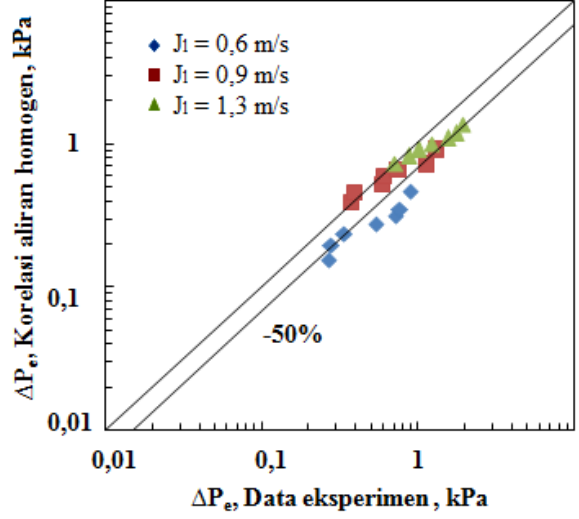


Figure 10. Pressure recovery $\Delta P_{e, exp}$ as a function of gas quality

Table 3. Standard deviation between pressure recovery research results and equations

Deviation	The homogeneous	Wadle
	flow method	correlation
	equation	(1988)
The mean of	0,24 kPa	0,35 kPa
deviation value		
Standard	0,32 kPa	0,43 kPa
deviation (S)		



(a) The homogeneous flow method correlation

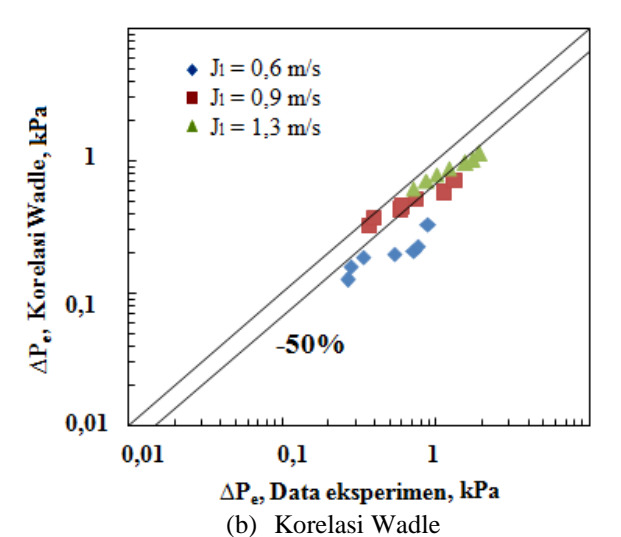


Figure 11. Comparison of experimental ΔP_e values to calculations

Pressure recovery results were compared to results which were obtained of the homogeneous flow Wadle correlation (1988). method and comparison graph is shown in Figure 11. In this study, the homogeneous flow method gives a prediction using lower deviation value compared to the Wadle correlation (1988) shown in Table 3. The differences of the two correlations are based on the mixed mass density determination, mass flux as well as empirical constants which has been determined in the Wadle correlation (1988). At the superficial velocity variation of water 0.6 m/s can not be predicted well because the differential pressure transducer has a low accuracy on the condition.

CONCLUSION

From the data and analysis that has been done can be concluded as follows:

- 1. In this research, two-phase bubble, plug, and slug flow patterns were obtained. Wavy and annular flow patterns were not found in this study.
- 2. In this two-phase flow study, the pressure recovery value based on homogeneous flow method and Wadle correlation tend to be lower than pressure recovery research results.
- The comparison of Wadle correlation to the pressure recovery value based on homogeneous flow method gave a result that was closer to the pressure recovery research results.

REFERENCE

- Ahmed, W.H., Ching, C.Y., dan Shoukri, M. 2007. Pressure Recovery of Two-Phase flow Across Sudden Expansions, International Journal of Multiphase Flow, Vol. 33, hlm. 575-594.
- Ahmed, W.H., Ching, C.Y., dan Shoukri, M. 2007. Development of Two-phase Flow Downstream of a Horizontal Sudden Expansion, International Journal of Multiphase Flow, Vol. 29, hlm. 194-206.
- Chen, I. Y., Liu, C., Chien, K., Wang, C. 2008. Two-Phase flow Characteristics Across Sudden Expansion In Small Rectangular Channels, Experimental Thermal and Fluid Science, Vol. 32, hlm. 696-706.
- J.W., Garimella, S. Coleman, dan Characterization of Two-phase Flow Patterns in Small Diameter Round and Rectangular Tubes, International Journal of Heat and Mass Transfer, Vol. 31, hlm. 2869-2881.
- Huang, G., Ji, H., Huang, Z., Wang, B., dan Li, H. Flow Regime Identification of Mini-Pipe Gas-Liquid Two-Phase Flow Based on Textural Feature Series, National Natural Science Foundation of China.
- Ide, H. dkk. 2007. Fundamental Data on the Gas-Liquid Two-Phase Flow in Minichannels, International Journal of Thermal Sciences, Vol. 46, hlm. 519-530.
- Kandlikar, S., Garimella, S., Li, D., Colin, S., dan King, M.R. 2006. Heat Transfer and Fluid Flow in Minichannels and Michrochannels, India.
- Koestoer, R.I., dan Proborini, S. 1994. Aliran Dua Fase dan Fluks Kalor Kritis, Pradya Paramita, Jakarta Timur.
- Mahendale, S.S., Jacobi, A.M., Ahah, R.K. 2000. Fluid Flow and Heat Transfer Micro- and Meso-scales with Aplication to Heat Exchanger Design, dalam Cheng, L., Mewes, D. 2005. Review of Two-Phase Flow and Flow Boiling of Mixtures in Small and Mini

- Channels, International Journal of Multiphase Flow, Vol. 32, hlm, 185-207.
- Mishima, K. dan Hibiki, T. Flow Regime two-phase rectangular channels, dalam flow in Kandlikar, S., Garimella, S., Li, D., Colin, S., dan King, M.R. 2006. Heat Transfer and Fluid Flow in Minichannels and Michrochannels, India.
- Munson, B.R., Young, D.F., dan Okhiisi, T.H. 2009. Fundamentals of Fluid Mechanics, John Wiley and Sons, United States of America.
- Supranto, J. 2000. Statistik: Teori dan Aplikasi, Erlangga, Jakarta.
- Venkatesan, M., Das, S.K., dan Balakrishnan, A.R. 2009. Effect of Tube Diameter on Two-Phase Flow Patterns in Mini Tube, The Canadian Journal Of Chemical Engineering, Vol. 88, hlm.936-944.
- Wadle, M. 1989. A New Formula For the Pressure Recovery in an Abrupt Diffusor, International Journal of Multiphase Flow, Vol. 15, hlm.
- Zhao, J.F. 2011. Flow Patterns, Pressure Drops and Other Related Topics of Two-phase Gas-liquid Flow in Microgravity, dalam Belmiloudi A. (ed.), Heat Transfer-Theoretical Analysis, Experimental and Industrial Systems, hlm.419-436, Intech, China.

NATURAL CONVECTION NUMERIC SIMULATION ON METAL FREEZING USING **DIFFERENTIAL METHOD**

Heri Suprianto¹, Eko Prasetyo B.², Purwadi Joko Widodo²

¹Student, ²Lecturer– Mechanical Engineering Department–Universitas Sebelas Maret

Keywords:

Abstract:

natural convection metal solidification finite different method rayleigh number

The research of modeling of natural convection in metal solidification process with finite different method was conducted to determine temperature distribution and fluid flow profil with variations value Rayleigh number. The research conducted by solving governing equation of natural convection with finite difference approximation. Governing equation of natural convection consist of continuity equation, momentum equations, and energy equation. The ADI (Alternating Directional Implicit) method was used to discriteze for governing equation of natural convection. Finite difference method was written in Fortran language whereas the temperature distribution and fluid flow profile were visualized with Matlab software. The results of this research was validated by comparing the results obtained with Rajiv Sampath research. Comparison of the results of research showed good agreement. The result showed that solidification process occurs faster at Ra 10⁴ compared with 10⁵ and 10⁶

1. INTRODUCTION

Numerous things related to the heat transfer are found in everyday life, especially in the field of industry. Heat transfer can occur in three ways, namely conduction, convection, and radiation.

Convection is a heat transfer that occurs between solid surface to the moved fluid which caused by the temperature difference within. Convection which is based on the fluid flow origins are categorized into two categories, namely the forced convection and natural convection.

Forced Convection is heat transfer fluid flow convection which happened influenced by external tools, such as fans, pumps, and others. While natural convection is heat transfer fluid flow convection which is caused by the differences in fluid density caused by heating and cooling.

Natural convection plays an important role in the engineering industry, one of them in the metal solidification process. Research which concerned on natural convection freezing problem is extremely crucial, because the fluid flow which caused by natural convection in liquid state, it changing the shape of the liquid/ solid interface and temperature distribution during freezing (Yinheng, 1994).

Physical phenomena that control the solid/ liquid interface shape during freezing are becoming necessary in numerous industrial processes. Its main characteristic is that the interface moves to separate the two phases with different physical properties. Differences in temperature cause the buoyancy liquid produces significant convection currents. Natural convection has a major influence on the morphology of its interface, freezing rate, and temperature distribution (Mohammad 2009).

Research about the natural convection issue of metals freezing has been carried out both experimental and numerically. Experimental laboratory research requires a significant financial cost and the process is quite complicated. Therefore, numerically study was developed which much cheaper. Various methods of numerical approach to determine the natural convection phenomenon has been done, using a mathematical model of the continuity equation, momentum equation, and energy equation.

Numerical study on natural convection issue of metal freezing was growing rapidly from year to year. McDaniel and Zabaras (1994) made a 2D numerical modeling on the basis of natural convection phase transformation on the issues of freezing and thawing of pure metals using the finite element method. Chen and Yoo (1995) analyzed the natural convection of aluminum freezing process by applying finite element method. Sampath and Zabaras (1999) created 2D and 3D numerical modeling on it utilizing the finite element method. Sampath and Zabaras research studied it on pure metals and alloys. Mohammad (2010) examined the numerical simulations in freezing water in a square mold in natural convection by employing finite volume method. Balhamadia, Kane, and Fortin (2012) made a phase transition modeling by natural convection in the water freezing and thawing gallium.

2. SCOPE

This study is aimed to make a natural convection modeling in the metal solidification process with finite difference methods. The velocity vector and temperature distribution were included.

3. LITERATURE REVIEW

McDaniel and Zabaras (1994) made a 2D numerical modeling on the basis of natural convection phase transformation on the freezing and thawing issues of pure metal using the finite element method. There were two cases analyzed. It was 105 and 106 of Rayleigh numbers. The boundary conditions that used were top, bottom, and right side insulation while the left side was the convection.

Chen and Yoo (1995) analyzed the freezing process aluminum in natural convection with the finite element method.

Sampath and Zabaras (1999) created 2D and 3D numerical modeling on the basis of natural convection phase transformation using the finite element method. Sampath and Zabaras Research investigated the freezing and thawing problem of pure metals and alloys. Basically, this study was continued by Zabaras research (1994).

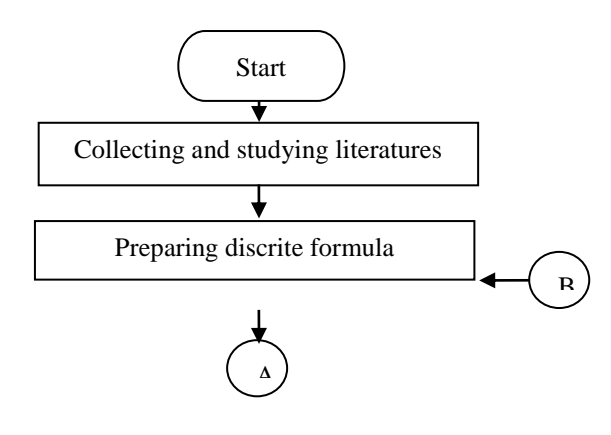
Mohammad (2010) studied the numerical simulations in freezing water in a square mold in natural convection by using finite volume method. Balhamadia, Kane, and Fortin (2012) fabricated the phase transition modeling by natural convection in the water freezing and thawing gallium.

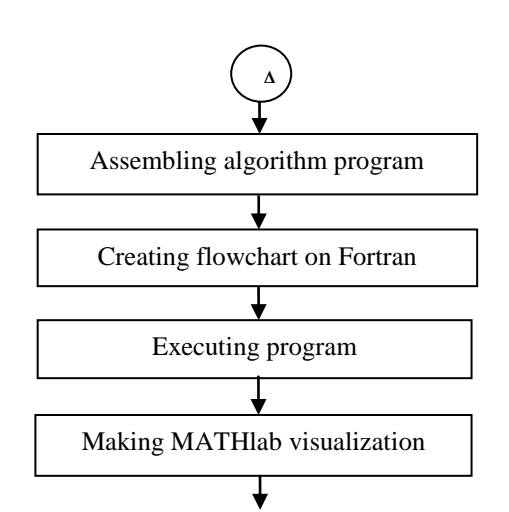
4. RESEARCH METHODOLOGY

4.1 Research Procedure

Research was done by making the program implementation to resolve the momentum equation, energy equation, and the continuity equation with the ADI method.

An outline of the research can be made following flow chart:





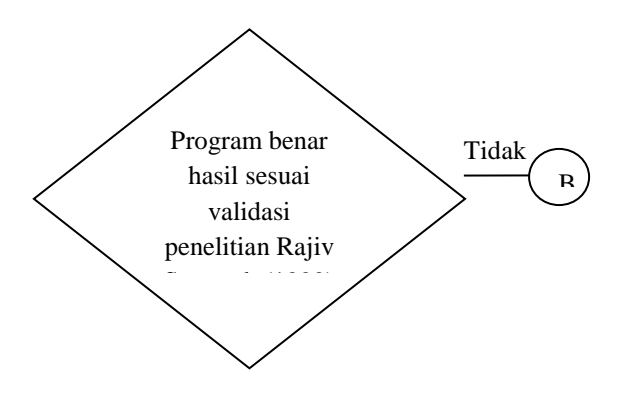


Figure 4.1. Research flowchart

4.2 Diskritisasi Persamaan Atur

Natural convection equation set consists of the continuity equation, momentum equation, and energy equation. In order to set the natural convection equations can be applied in the programming language. Firstly, discretization equation set was set up.

This study implementation, the discretization equation solved by the method set ADI. By defining $\frac{1}{2}(x_{i,j}^n+x_{i+1,j}^n)=XR$, $\frac{1}{2}(x_{i,j}^n+x_{i-1,j}^n)=XL$, $\frac{1}{2}(x_{i,j}^n+x_{i,j+1}^n)=XT$, $\frac{1}{2}(x_{i,j}^n+x_{i,j-1}^n)=XB$ where x is unknown variable (such as, u, v, and θ).

4.2.1 Momentum Equation Discrete4.2.1.1 X-axis Momentum Equation

Discretization of momentum equation used x-axis momentum equation x direction without including the pressure element. Therefore, the equation becomes:

$$\frac{\partial u}{\partial t} + u \frac{\partial u}{\partial x} + v \frac{\partial u}{\partial y} = \frac{Pr}{Ra^{0.5}} \left(\frac{\partial^2 u}{\partial x^2} + \frac{\partial^2 u}{\partial y^2} \right) + Pr\theta \cos \emptyset$$

For example $=\frac{Pr}{Ra^{0.5}}$, so, the equation above become,

$$\frac{\partial u}{\partial t} + u \frac{\partial u}{\partial x} + v \frac{\partial u}{\partial y} = A \left(\frac{\partial^2 u}{\partial x^2} + \frac{\partial^2 u}{\partial y^2} \right) + Pr\theta \cos \emptyset$$

X-sweep equation for momentum equation x-axis is

$$\frac{\partial \mathbf{u}}{\partial \mathbf{t}} + \mathbf{u} \frac{\partial \mathbf{u}}{\partial \mathbf{x}} + \mathbf{A} \frac{\partial^2 \mathbf{u}}{\partial \mathbf{x}^2} = -\mathbf{v} \frac{\partial \mathbf{u}}{\partial \mathbf{y}} + \mathbf{A} \frac{\partial^2 \mathbf{u}}{\partial \mathbf{y}^2} + \mathbf{Pr}\theta \cos \mathbf{0}$$

Discretization for each equation above can be explained:

$$\bullet \quad u \frac{\partial u}{\partial x} = \frac{1}{2\Delta x} \left[UR. u_{i+1,j}^{n+1/2} + (UR-UL) u_{i,j}^{n+1/2} + UL. u_{i-1,j}^{n+1/2} \right]$$

$$\frac{\partial^2 \mathbf{u}}{\partial \mathbf{x}^2} = \frac{\mathbf{u}_{i+1,j}^{n+1/2} - 2\mathbf{u}_{i,j}^{n+1/2} + \mathbf{u}_{i-1,j}^{n+1/2}}{\Delta \mathbf{x}^2}$$

$$\frac{\partial^2 \mathbf{u}}{\partial \mathbf{y}^2} = \frac{\mathbf{u}_{i,j+1}^{\mathbf{n}} - 2\mathbf{u}_{i,j}^{\mathbf{n}} + \mathbf{u}_{i,j-1}^{\mathbf{n}}}{\Delta \mathbf{y}^2}$$

By substituting equations above and multiplying with

$$u_{i,j}^{n+1/2} - u_{i,j}^{n} + \frac{\Delta t}{4\Delta x} \Big[UR.u_{i+1,j}^{n+1/2} + (UR-UL)u_{i,j}^{n+1/2} + UL.u_{i-1,j}^{n+1/2} \Big]$$

$$-\frac{A\Delta t}{2\Delta x^2} \! \left[u_{i+1,j}^{n+1/2} \! - \! 2 u_{i,j}^{n+1/2} \! + \! u_{i-1,j}^{n+1/2} \right] \! \! = \! \! - \frac{\Delta t}{2\Delta y} \left[VT.UT\text{-}VB.UB \right]$$

$$+\frac{A\Delta t}{2\Delta y^2} \Big(u_{i,j+1}^n \text{-} 2u_{i,j}^n \text{+} u_{i,j-1}^n\Big) + \frac{\Delta t}{2} \text{Pr.}\theta.\text{cos}\emptyset$$

Therefore those equations, would be collected into unknown variable on left side and known variable on

$$\begin{split} &u_{i\text{-}1,j}^{n+1/2} \left[\frac{\Delta t}{4\Delta x} \text{UL-} \frac{A\Delta t}{2\Delta x^2} \right] + u_{i,j}^{n+1/2} \left[1 + \frac{\Delta t}{4\Delta x} \left(\text{UR-UL} \right) + \frac{A\Delta t}{2\Delta x^2} \right] \\ &= u_{i,j}^n - \frac{\Delta t}{2\Delta y} \left(\text{VT.UT-VB.UB} \right) + \frac{A\Delta t}{2\Delta y^2} \left(u_{i,j+1}^n - 2u_{i,j}^n + u_{i,j-1}^n \right) \\ &+ \frac{\Delta t}{2} \text{Pr.}\theta.\text{cos}\emptyset \end{split}$$

Arrangement above idencally with equation $a_i \mathbf{u}_{\mathbf{i}+1,\mathbf{j}}^{\mathbf{n}+1/2} + b_i \mathbf{u}_{\mathbf{i},\mathbf{j}}^{\mathbf{n}+1/2} + c_i \mathbf{u}_{\mathbf{i}-1,\mathbf{j}}^{\mathbf{n}+1/2} = d_i$ with components $a_i, b_i,$ c_i and d_i each is tridiagonal matrix components

$$\begin{split} a_i &= \frac{\Delta t}{2\Delta x} \left[\frac{UL}{2} + \frac{A}{\Delta x} \right] \\ b_i &= \left[1 + \frac{\Delta t}{4\Delta x} \left(UR \text{-}UL \right) + \frac{A\Delta t}{2\Delta x^2} \right] \\ c_i &= \frac{\Delta t}{2\Delta x} \left[\frac{UR}{2} - \frac{A}{\Delta x} \right] \\ d_i &= u_{i,j}^n - \frac{\Delta t}{2\Delta y} \left(VT.UT\text{-}VB.UB \right) \\ &+ \frac{A\Delta t}{2\Delta y^2} \left(u_{i,j+1}^n \text{-} 2u_{i,j}^n + u_{i,j-1}^n \right) + \frac{\Delta t}{2} Pr.\theta.cos\emptyset \end{split}$$

b. Y-Sweep

Y-sweep equation for momentum equation y-axis is:

$$\frac{\partial \mathbf{u}}{\partial t} + \mathbf{v} \frac{\partial \mathbf{u}}{\partial \mathbf{x}} + \mathbf{A} \frac{\partial^2 \mathbf{u}}{\partial \mathbf{v}^2} = -\mathbf{u} \frac{\partial \mathbf{u}}{\partial \mathbf{v}} + \mathbf{A} \frac{\partial^2 \mathbf{u}}{\partial \mathbf{x}^2} + \mathbf{Pr} \theta \cos \emptyset$$

Discretization for each equation above can be

$$\frac{\partial^2 u}{\partial v^2} = \frac{u_{i+1,j}^{n+1} - 2u_{i,j}^{n+1} + u_{i-1,j}^{n+1}}{\Delta v^2}$$

By substituting equations above and multiplying with $\frac{\Delta t}{2}$, can be obtained matrix tridiagonal coefficient:

$$\begin{array}{l} \bullet \quad v \frac{\partial u}{\partial y} = \frac{1}{\Delta y} \left[VT.UT-VB.UB \right] \\ \bullet \quad \frac{\partial^2 u}{\partial y^2} = \frac{u^n_{i,j+1} \cdot 2u^n_{i,j} + u^n_{i,j-1}}{\Delta y^2} \\ \text{By substituting equations above and multiplying with} \\ \frac{\Delta t}{2}, \text{ can be obtained:} \\ u^{n+1/2}_{i,j} - u^n_{i,j} + \frac{\Delta t}{4\Delta x} \left[UR.u^{n+1/2}_{i+1,j} + (UR-UL)u^{n+1/2}_{i,j} + UL.u^{n+1/2}_{i-1,j} \right] \\ -\frac{A\Delta t}{2\Delta x^2} \left[u^{n+1/2}_{i+1,j} - 2u^{n+1/2}_{i,j} + u^{n+1/2}_{i-1,j} \right] = -\frac{\Delta t}{2\Delta y} \left[VT.UT-VB.UB \right] \\ +\frac{A\Delta t}{2\Delta x^2} \left(u^{n+1/2}_{i,j-1} - 2u^{n+1/2}_{i,j-1} + u^{n+1/2}_{i,j-1} \right) + \frac{\Delta t}{2} \Pr.\theta.\cos\emptyset$$

4.2.1.2 Y-axis Momentum Equation

Discretization of momentum equation used y-axis momentum equation y direction without including the pressure element. Therefore, the equation becomes:

$$\frac{\partial \mathbf{v}}{\partial t} + \mathbf{u} \frac{\partial \mathbf{v}}{\partial \mathbf{x}} + \mathbf{v} \frac{\partial \mathbf{v}}{\partial \mathbf{y}} = \frac{\Pr}{\mathbf{R}\mathbf{a}^{0.5}} \left(\frac{\partial^2 \mathbf{v}}{\partial \mathbf{x}^2} + \frac{\partial^2 \mathbf{v}}{\partial \mathbf{y}^2} \right) + \Pr\theta\cos\emptyset$$

For example $A = \frac{Pr}{Ra^{0.5}}$, so, the equation above becomes:

$$\frac{\partial \mathbf{v}}{\partial \mathbf{t}} + \mathbf{u} \frac{\partial \mathbf{v}}{\partial \mathbf{x}} + \mathbf{v} \frac{\partial \mathbf{v}}{\partial \mathbf{y}} = \mathbf{A} \left(\frac{\partial^2 \mathbf{v}}{\partial \mathbf{x}^2} + \frac{\partial^2 \mathbf{v}}{\partial \mathbf{v}^2} \right) + \mathbf{Pr} \theta \cos \emptyset$$

X-Sweep

X-sweep equation for momentum equation x-axis is:

$$\frac{\partial \mathbf{v}}{\partial t} + \mathbf{u} \frac{\partial \mathbf{v}}{\partial x} + \mathbf{A} \frac{\partial^2 \mathbf{v}}{\partial x^2} = -\mathbf{v} \frac{\partial \mathbf{v}}{\partial y} + \mathbf{A} \frac{\partial^2 \mathbf{v}}{\partial y^2} + \mathbf{Pr}\theta \cos \emptyset$$

Discretization for each equation above can be explained:

•
$$u \frac{\partial v}{\partial x} = \frac{1}{2\Delta x} \left[UR.v + \left(UR-UL \right) v_{i,j}^{n+1/2} + UL.v_{i-1,j}^{n+1/2} \right]$$

$$\frac{\partial^2 \mathbf{v}}{\partial \mathbf{x}^2} = \frac{\mathbf{v}_{i+1,j}^{n+1/2} - 2\mathbf{v}_{i,j}^{n+1/2} + \mathbf{v}_{i-1,j}^{n+1/2}}{\Delta \mathbf{x}^2}$$

$$v \frac{\partial v}{\partial y} = \frac{1}{\Delta y} \left[V T^2 - V B^2 \right]$$

$$\stackrel{?}{ } \frac{\partial^2 \mathbf{v}}{\partial \mathbf{v}^2} = \frac{\mathbf{v}_{i,j+1}^n - 2\mathbf{v}_{i,j}^n + \mathbf{v}_{i,j-1}^n}{\Delta \mathbf{v}^2}$$

By substituting equations above and multiplying with $\frac{\Delta t}{2}$, can be obtained: tridiagonal matrix coefficient:

$$\begin{split} &a_{i} = \frac{\Delta t}{2\Delta x} \left[\frac{UL}{2} + \frac{A}{\Delta x} \right] \\ &b_{i} = \left[1 + \frac{\Delta t}{4\Delta x} \left(UR\text{-}UL \right) + \frac{A\Delta t}{2\Delta x^{2}} \right] \\ &c_{i} = \frac{\Delta t}{2\Delta x} \left[\frac{UR}{2} - \frac{A}{\Delta x} \right] \\ &d_{i} = v_{i,j}^{n} - \frac{\Delta t}{2\Delta y} \left(VT^{2}\text{-}VB^{2} \right) \\ &+ \frac{A\Delta t}{2\Delta y^{2}} \left(v_{i,j+1}^{n} - 2v_{i,j}^{n} + v_{i,j-1}^{n} \right) + \frac{\Delta t}{2} Pr.\theta.cos\emptyset \end{split}$$

b. Y-Sweep

Y-sweep equation for momentum equation y-axis is:

$$\frac{\partial \mathbf{v}}{\partial t} + \mathbf{v} \frac{\partial \mathbf{v}}{\partial x} + \mathbf{A} \frac{\partial^2 \mathbf{v}}{\partial \mathbf{v}^2} = -\mathbf{u} \frac{\partial \mathbf{v}}{\partial y} + \mathbf{A} \frac{\partial^2 \mathbf{v}}{\partial x^2} + \mathbf{Pr} \theta \cos \emptyset$$

Discretization for each equation above can be

$$\frac{\partial^2 \mathbf{v}}{\partial \mathbf{x}^2} = \frac{\mathbf{v}_{i,j+1}^{n+1/2} - 2\mathbf{v}_{i,j}^{n+1/2} + \mathbf{v}_{i,j-1}^{n+1/2}}{\Delta \mathbf{x}^2}$$

By substituting equations above and multiplying with $\frac{\Delta t}{2}$, can be obtained matrix tridiagonal coefficient:

$$\begin{split} &a_{j} = \frac{\Delta t}{2\Delta y} \left[\frac{VB}{2} + \frac{A}{\Delta x} \right] \\ &b_{j} = \left[1 + \frac{\Delta t}{4\Delta y} \left(VT - VB \right) + \frac{A\Delta t}{2\Delta y^{2}} \right] \\ &c_{j} = \frac{\Delta t}{2\Delta y} \left[\frac{VB}{2} - \frac{A}{\Delta y} \right] \\ &d_{i} = u_{i,j}^{n+1/2} - \frac{\Delta t}{2\Delta x} \left(UR.VR - UL.VL \right) \\ &+ \frac{A\Delta t}{2\Delta x^{2}} \left(v_{i,j+1}^{n+1/2} - 2v_{i,j}^{n+1/2} + v_{i,j-1}^{n+1/2} \right) + \frac{\Delta t}{2} \Pr.\theta.\cos\emptyset \end{split}$$

4.2.2 Pressure Iteration Using Line Gauss Seidel

Formula was used to calculate pressure is:

$$\frac{\partial^2 \mathbf{p}}{\partial \mathbf{x}^2} + \frac{\partial^2 \mathbf{p}}{\partial \mathbf{y}^2} = \frac{1}{\Delta t} \left(\frac{\partial \mathbf{u}}{\partial \mathbf{x}} + \frac{\partial \mathbf{v}}{\partial \mathbf{y}} \right)$$

Dicretization for each equations above:

$$\frac{\partial^2 p}{\partial v^2} = \frac{p_{i,j+1} - 2p_{i,j} + p_{i,j-1}}{\Delta v^2}$$

By substituting equations above, so tridiagonal matrix coefficient can be obtained:

$$a_i=1$$

 $b_i=-4$

$$d_{i} = -p_{i,j+1} - p_{i,j-1} + \frac{\Delta x^{2}}{\Delta t} \left[\frac{u_{i+1,j} - u_{i-1,j}}{2\Delta x} + \frac{v_{i+1,j} - v_{i-1,j}}{2\Delta v} \right]$$

Energy Discretization Equation

Energy discretization equation was used:

$$\frac{\partial \theta}{\partial t} + u \frac{\partial \theta}{\partial x} + v \frac{\partial \theta}{\partial y} = \frac{1}{Ra^{0.5}} \left(\frac{\partial^2 \theta}{\partial x^2} + \frac{\partial^2 \theta}{\partial y^2} \right)$$

For example $=\frac{1}{Ra^{0.5}}$, so, the equation becomes:

$$\frac{\partial \theta}{\partial t} + u \frac{\partial \theta}{\partial x} + v \frac{\partial \theta}{\partial y} = B \left(\frac{\partial^2 \theta}{\partial x^2} + \frac{\partial^2 \theta}{\partial y^2} \right)$$

discretization:

a. X-Sweep

X-sweep equation for momentum equation x-axis is

$$\frac{\partial \theta}{\partial t} + u \frac{\partial \theta}{\partial x} + B \frac{\partial^2 \theta}{\partial x^2} = -v \frac{\partial \theta}{\partial y} + B \frac{\partial^2 \theta}{\partial y^2}$$

Discretization for each equation above can be explained:

$$\begin{array}{ll} & \quad \text{u} \frac{\partial \theta}{\partial x} = \frac{1}{2\Delta x} \left[UR. \theta_{i+1,j}^{n+1/2} + \left(UR-UL \right) \theta_{i,j}^{n+1/2} + UL. \theta_{i-1,j}^{n+1/2} \right] \\ & \quad \text{\star} \quad \frac{\partial^2 \theta}{\partial x^2} = \frac{\theta_{i+1,j}^{n+1/2} - 2\theta_{i,j}^{n+1/2} + \theta_{i-1,j}^{n+1/2}}{\Delta x^2} \end{array}$$

$$\frac{\partial^2 \theta}{\partial x^2} = \frac{\theta_{i+1,j}^{n+1/2} - 2\theta_{i,j}^{n+1/2} + \theta_{i-1,j}^{n+1/2}}{\Delta x^2}$$

$$v \frac{\partial x^2}{\partial y} = \frac{1}{\Delta y} \left[VT.\theta T - VB.\theta B \right]$$

By substituting equations above and multiplying with $\frac{\Delta t}{2}$, can be obtained: tridiagonal matrix coefficient:

$$\begin{split} &a_{i} \!=\! \frac{\Delta t}{2\Delta x} \! \left[\! \frac{UL}{2} \! + \! \frac{B}{\Delta x} \! \right] \\ &b_{i} \! =\! \left[1 \! + \! \frac{\Delta t}{4\Delta x} \left(UR \! - \! UL \right) \! + \! \frac{B\Delta t}{2\Delta x^{2}} \right] \\ &c_{i} \! =\! \frac{\Delta t}{2\Delta x} \! \left[\! \frac{UR}{2} \! - \! \frac{B}{\Delta x} \right] \\ &d_{i} \! =\! \theta_{i,j}^{n} \! - \! \frac{\Delta t}{2\Delta y} \left(VT \! \cdot \! \theta T \! - \! VB \! \cdot \! \theta B \right) \! + \! \frac{B\Delta t}{2\Delta y^{2}} \left(\theta_{i,j+1}^{n} \! - \! 2\theta_{i,j}^{n} \! + \! \theta_{i,j-1}^{n} \right) \end{split}$$

b. Y-Sweep

Y-sweep equation for momentum equation y-axis is

$$\frac{\partial \theta}{\partial t} + v \frac{\partial \theta}{\partial x} + B \frac{\partial^2 \theta}{\partial x^2} = -u \frac{\partial \theta}{\partial y} + B \frac{\partial^2 \theta}{\partial y^2}$$

Y-sweep equation for momentum equation y-axis is:

$$u \frac{\partial \theta}{\partial x} = \frac{1}{\Lambda x} \left[UR.\theta R-UL.\theta L \right]$$

By substituting equations above and multiplying with $\frac{\Delta t}{2}$, can be obtained matrix tridiagonal coefficient::

$$\begin{split} a_i &= \frac{\Delta t}{2\Delta y} \left[\frac{UL}{2} + \frac{B}{\Delta y} \right] \\ b_i &= \left[1 + \frac{\Delta t}{4\Delta y} \left(VT \text{-}VB \right) + \frac{B\Delta t}{2\Delta y^2} \right] \\ c_i &= \frac{\Delta t}{2\Delta y} \left[\frac{VB}{2} - \frac{B}{\Delta y} \right] \\ d_i &= \theta_{i,j}^{n+1/2} - \frac{\Delta t}{2\Delta x} \left(UR.\theta R \text{-}UL.\theta L \right) \\ &\quad + \frac{B\Delta t}{2\Delta x^2} \left(\theta_{i,j+1}^{n+1/2} - 2\theta_{i,j}^{n+1/2} + \theta_{i,j-1}^{n+1/2} \right) \end{split}$$

5. RESULT AND DISCUSSION

5.1 Program Validation

Validation program was done by comparing the current research to the Rajiv Sampath research (1999). Rajiv Sampath research domain (1999) was the resolution of natural convection case in metal solidification process on a square mold with 1: 1 of aspect ratio, with the walls below, above, and right side condition were insulating, while the left Wall was convection.

$$\frac{\partial \theta}{\partial y} = 0$$

$$\frac{\partial p}{\partial y} = 0$$

$$\frac{\partial p}{\partial x} = 0$$

$$\theta = 0.5 \qquad \frac{\partial p}{\partial x} = 0$$

$$\frac{\partial \rho}{\partial x} = 0$$

$$\frac{\partial \rho}{\partial y} = 0$$

$$\frac{\partial \rho}{\partial y} = 0$$

Figure 5.1 Boundary and require research condition

Rajiv Sampath research (1999) was using finite element method with the same boundary conditions to the present study boundary conditions. Isothermal visualization and velocity vector results will be compared with Rajiv Sampath research (1999) at Ra = 105. Isothermal comparison results is shown in following Table 4.1. and Table 4.2:

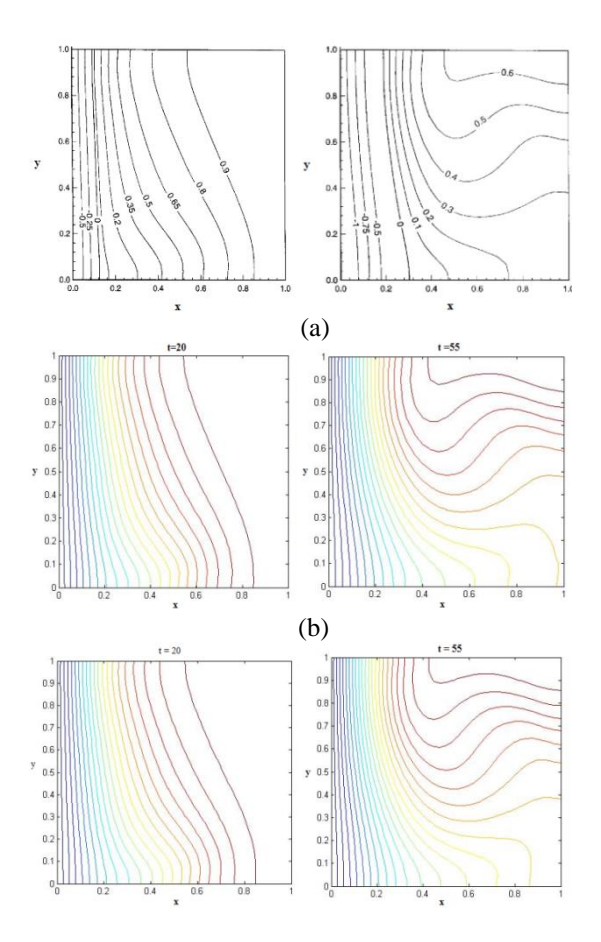
Table 4. 1. Isotermal comparison result at t=20

Titik		Sekarang		Beda		Beda (%)	
x	Y	Grid 61x61	Grid 81x81	(%)	Sampath	61x61	81x81
0.53	0.1	0.52931	0.50247	5.342	0.5	5.862	0.494
0.5	0.3	0.65937	0.65371	0.866	0.65	1.442	0.571
0.7	0.2	0.82506	0.81854	0.797	0.8	3.133	2.318
0.8	0.3	0.92896	0.92603	0.316	0.9	3.218	2.892

Table 4.2. Isotermal comparison result at t=55

Titik		Sekarang		Beda		Beda (%)	
x	Y	Grid 61x61	Grid 81x81	(%)	Sampath	61x61	81x81
0.6	0.3	0.30965	0.30485	1.575	0.3	3.217	1.617
1.0	0.63	0.41458	0.39613	4.658	0.4	3.645	0.968
0.4	0.68	0.5161	0.50969	1.258	0.5	3.22	1.938
1.0	0.87	0.61367	0.60215	1.913	0.6	2.278	0.358

Isothermal comparison results between the current study to Sampath research above shows good accuracy with 5862 for the 61x61 grid and 2892 for 81x81 of a maximum error. It shows for the 81x81 grid has a maximum error value is smaller than the 61x61 grid, so that in this study we used the 81x81 grid. Visualization comparison of nowdays research with Sampath research above can be shown in the following figure:



(c)
Figure 5.2 Isotermal visualization comparison at Ra=10⁵ (a) Rajiv Sampath research (1999) (b)
Nowdays research with 61x61 grid (c) with 81x81 grid

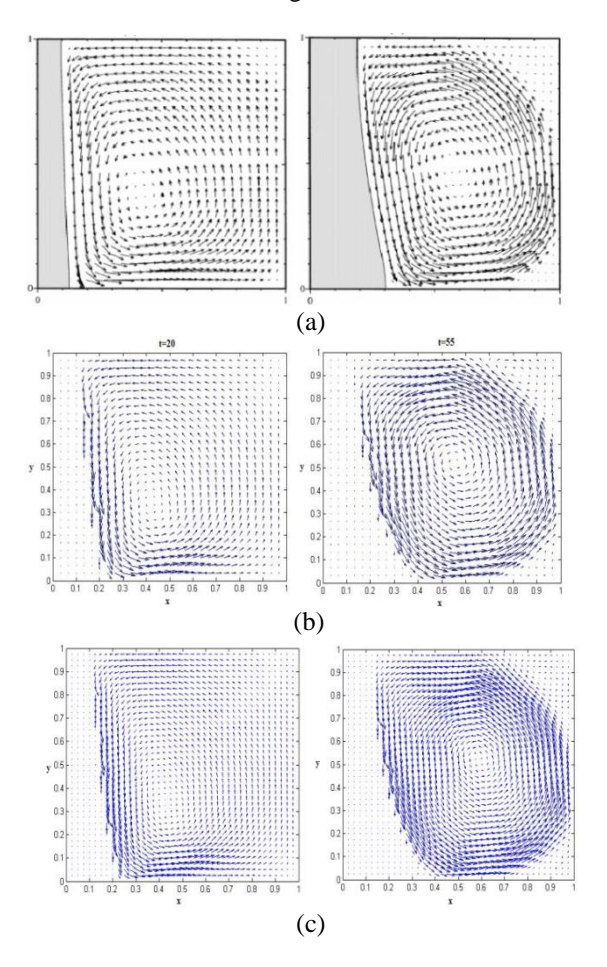


Figure 5.3. Visualization comparison velocity vector at Ra=10⁵ (a) Rajiv Sampath research (1999) (b) Nowdays research with 61x61 grid (c) with 81x81 grid

Visually, nowadays research shows similarities of flow temperature distribution and velocity with Rajiv Sampath study (1999). Thereforem, it can be said using the finite difference method has a good fit.

5.2 Natural Convection Simulation on Metal Solidification Process

Natural convection simulation cases on metal solidification process on a square mold is shown with the 81x81 grid, 0.0149 of Prandlt number (Pr), and dt= 0.001 of time step, and Rayleigh number (Ra) variations were 104.105 and 106. The simulation results can be seen in the following image:

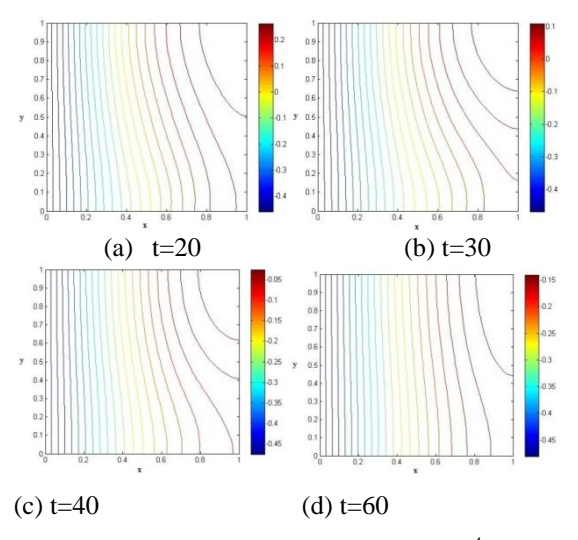


Figure 5.4. Isotermal on $Ra = 10^4$

Temperature tranformation can be seen in the temperature distribution graph which represented by a point (x, 0.1), wherein x were 0.1, 0.2, 0.3, 0.4, 0.5, 0.6, 0.7, 0.8, 0.9, and 1. A temperature distribution graph is as follows:

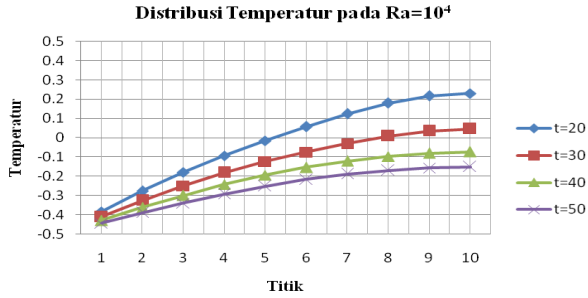


Figure 5.5. Temperature distribution at Ra= 10⁴

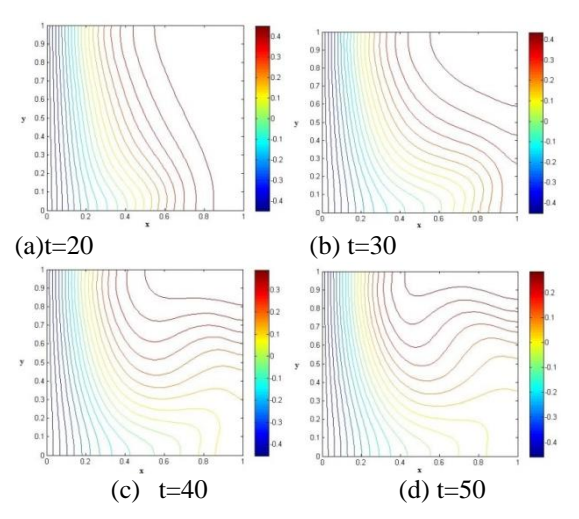


Figure 5.6. Isotermal at Ra= 10⁵

Temperature distribution can be seen in the temperature distribution graph which performed by a point (x, 0.1), wherein x is 0.1, 0.2, 0.3, 0.4, 0.5, 0.6, 0.7, 0.8, 0.9, and 1. Temperature distribution graph is as follows:

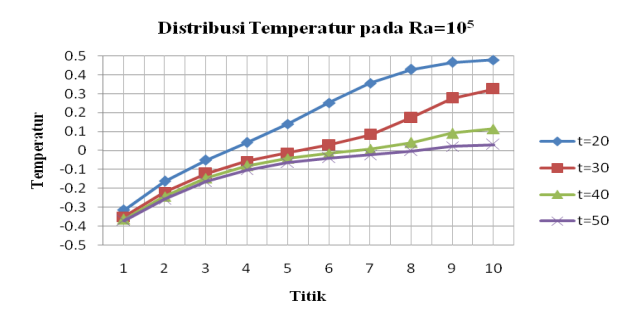


Figure 5.7. Temperature distribution at $Ra = 10^5$

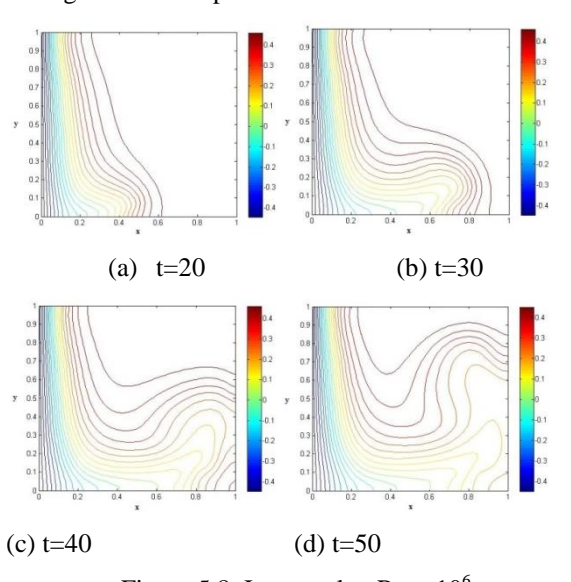


Figure 5.8. Isotermal at $Ra = 10^6$

Temperature transformation can be seen in the temperature distribution graph which served by a point (x, 0.1), wherein x is 0.1, 0.2, 0.3, 0.4, 0.5, 0.6, 0.7, 0.8, 0.9, and 1. Temperature distribution graph is as follows:

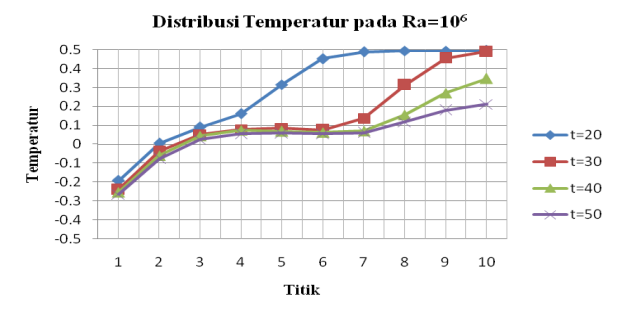


Figure 5.9. Temperature distribution at $Ra = 10^6$

Isothermal plot results in Figure 4.4, Figure 4.6, and Figure 4.8 portrays the temperature distribution visually. Figure 4.4 at Ra = 104 displays that the cold fluid moves down and the hot fluid moving upwards. Cold fluid movement influenced their gravity and density changes due to its temperature changes which is producing the density increased, while the hot fluid movement was affected by buoyant force because it has a smaller density than the cold fluid. Fluid temperature near the left wall was strongly influenced by the ambient temperature.

This also occured on Ra= 105 and 106 which shown in Figure 4.6 and Figure 4.8. Isothermal figure which can be seen that the fluid movement on the wall to get the cooling fluid densit will be increased. The fluid density escalation caused the fluid to move downwards, while the fluid has a lower density will move upwards. Fluid movement downward was also influenced by gravity however fluid movement upward influenced by their buoyancy occurs due to it has a smaller density.

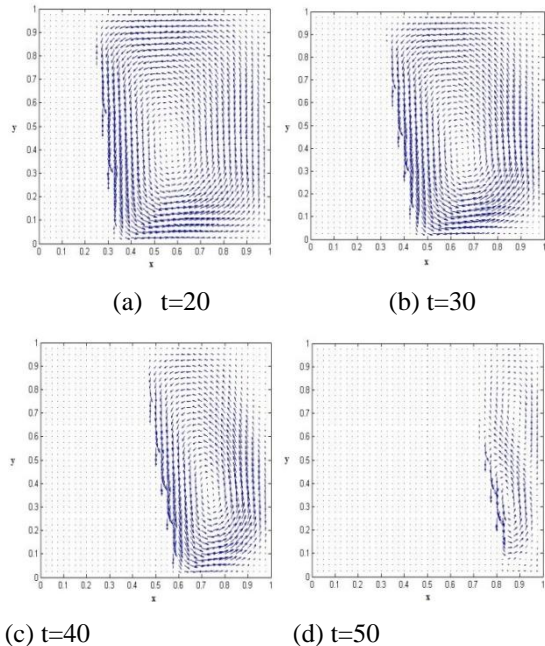


Figure 5.10. Velocity vector at $Re=10^4$

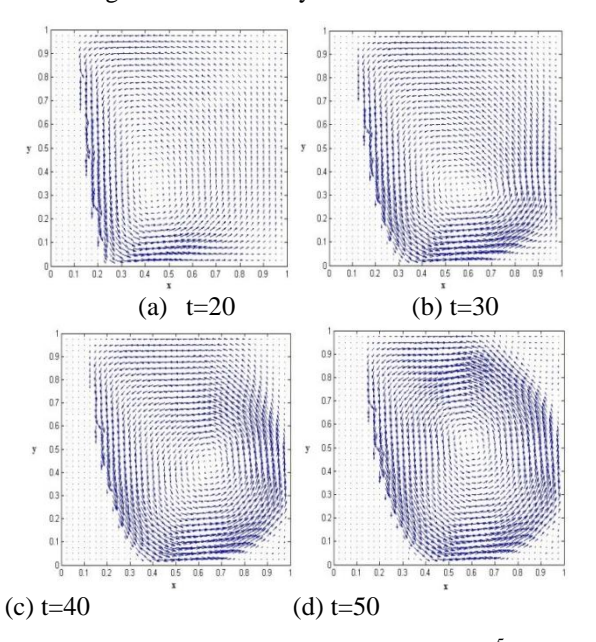


Figure 5.11. Velocity vector at Ra= 10⁵

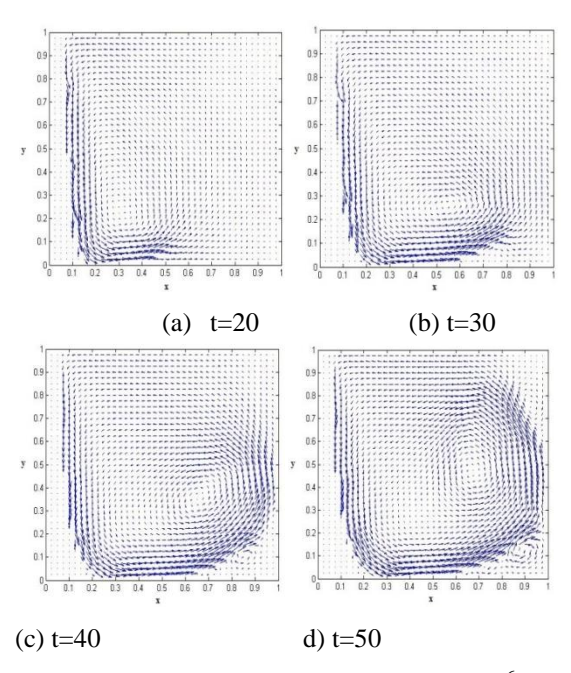


Figure 5.12. Velocity vector at $Ra = 10^6$

Velocity vector visual results with the velocity vector variation can be seen in Figure Ra 4:10 to 4:12. It portrays that the fluid movement opposite to clockwise and freezing the bottom left looks faster. It also illustrates that the cold fluid moves down and the hot fluid moving upwards. Cold fluid movement was influenced by their gravity and density changes due to its temperature changes which was generated by density increased, while hot fluid movement was affected by buoyancy force.

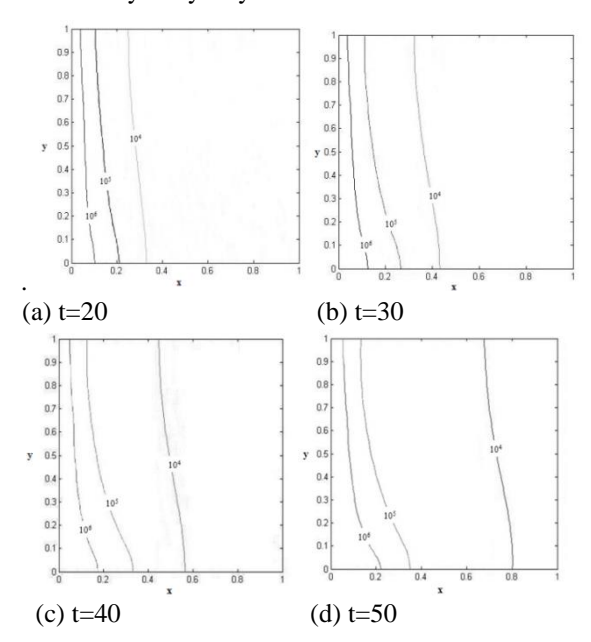


Figure 5.13. The initial solidification comparison

The initial solidification comparison which according to the Ra variations can be seen in Figure 4.13. It portrays that the initial freezing at Ra= 104 is faster than Ra= 105 and 106. It can be concluded that

rayleigh number greatly affects the freezing process, the greater rayleigh number the longer it will reverse the freezing process so shall.

6. Conclusion

From this research and discussion that has been done. It produced a numerous conclusions:

- a. Research comparison of Rajiv Sampath study (1999) for natural convection problem in metal solidification process on a square mold indicates that the method which was used in this study can provide acceptable results in those cases.
- b. Cold fluid moved down and the hot fluid moving upwards. Cold fluid movement was influenced by their gravity and density changes due to its temperature transformation which caused the density went up, while the movement of hot fluid was affected by Buoyancy force due to it has a smaller density than the cold fluid.
- c. Rayleigh number greatly affects the metal solidification speed. The smaller of Rayleigh, the faster the solidification process and the greater Rayleigh number clots more slowly.

7. Reference

Belhamadia, Y., Kane, A.S., Fortin, A., 2012, *An Enhanced Mathematical Model for Phase Change Problem With Natural Convection*, International Journal of Numerical Analysis and Modeling, Vol.3, 192-206.

Brandes, E.A., Brook, G.B., 1992, *Smithells Metals Reference Book*, *7th edition*, Butterworth-Heinemann, Oxford.

Cengel, A.Y., 2008, Heat Transfer A Practical Approach Second Edition, McGraw-Hill, New York. Chen, Y., Im, Y.T., Yoo, J., 1995, Finite Element Analaysis of Solidification of Aluminum with Natrural Convection, Journal of Material Processing Technology, Vol.52, 592-609, Elsevier.

Hoffman, K.A., 2000, Computation Fluid Dynamics For Engineering Volume I, Engineering System $^{\rm TM}$, Kansas USA.

Holman, J.P., 2010, *Heat Transfer Tenth Edition*, McGraw-Hill, New York.

Incropera, F.M., 1996, *Introduction to Heat Transfer*, John Wiley & Sons, USA.

McDaniel, D. J., Zabaras, N., 1994, A least-squares front-tracking finite element method analysis of phase change with natural convection, International Journal Numerical Method Engineering, Vol. 37, 2755-2777.

FIBER WEIGHT FRACTION EFFECT TO ACOUSTIC PROPERTIES OF rHDPE CANTULA COMPOSITE

M. Taufik Burhany Hendrowarsito¹, Wijang Wisnu Raharjo², Dwi Aries Himawanto² ¹Student, ²Lecturer– Mechanical Engineering Department–Universitas Sebelas Maret

Keywords:

Natural fiber composites, sound absorption coefficient, sound absorption material

Abstract:

In this study, composites made from recycled HDPE and Cantula fiber have been done and the absorption coefficient have been measured. Composites rHDPE-Cantula were made using hot press for approximately 60 minutes with 170°C temperature while pressure exerted by 50 bar. In this study the weight ratio of Cantula fiber was varied 40%, 50%, 60%, and 70%. Impedance Tube Method was used to measure the sound absorption coefficient in accordance with ASTM E 1050. An increase weight ratio wasn't influence the sound absorption coefficient significantly, but the optimum sound absorption coefficient shifted to the higher frequencies from 80-200 Hz. An increase weight ratio showed better sound absorption coefficient from 500-1600 Hz, but the result from 60% weight ratio showed low sound absorption coefficient that may caused by it high density leading to the reduction of porosity. This result was supported by density measurement in accordance with ASTM D 792, which the result showed that the sound absorption coefficient increase with decreasing of the density...

INTRODUCTION

Global industry, science, and technology development improved the quality of human life but also posed some problems for the environment and human health for instance noise pollution (Jayamani, 2013). Sound-absorbing material application has become one of the main requirements for obtaining human convenience today, especially in the automotive industry (Ekici, 2012). Vehicle panel development has begun to shift in natural fibers utilization which cost less, lightweight, and environmental friendly (Abdullah, 2011). Generally, natural fibers have the ability to absorb sound, especially for noise controlling at vehicles, offices, and industrial (Eriningsih, 2009).

Pure thermoplastic composites production as a matrix has been done by society. However, plastic application was continuously increased which causes plastic waste existence overflowed. Therefore, it needs treatments which regarding environmental pollution problems. It count 40% of 19.2 million tons was polyethylene, Lei, (2007) performed a study using High Density Polyethylene desolation (HDPE). Generally, it properties are chemical processes, temperature resistant, and stable against air oxidation (Gunawan, 2012). This indicates that it can be used as a matrix in composites manufacturing as a sound absorber, which it will be used in this study.

Noise adverse effects on humans are emotional disturbance, discomfort feeling, unstable blood pressure, headache, and less concentration (Eriningsih, 2009). Those problems can be anticipated by taking action to reduce noises using acoustic absorbers (Kartikaratri, 2012). Sound waves

energy will be absorbed by sound absorbing materials and turned it into the heat (Christian, 2014).

Recycle High Density Polyethylene (rHDPE) was used for a binder of cantula fiber which produces composites that are strong, lightweight, inexpensive, and environmental friendly. Fiber weight fraction optimization was this study main focus. It varied 40%, 50%, 60%, and 70% to determine the most excellent sound absorption performance.

RESEARCH METHODOLOGY

Materials and instruments:

Rincian peralatan yang digunakan dalam penelitian ini adalah

- a. Hot Press Machine
- b. Atomizer Machine
- c. Crusher Machine
- d. Scales
- e. Digital Termometer
- f. HDPE waste
- g. Cantulafibers

RHDPE Fiber Productions

HDPE waste which still bottle shaped was chopped using a crushing machine until it forms a powder. RHDPE powder atomizer inserted on a machine with 200°C of temperature ± 7 bar of pressure for 15 minutes to obtain a ready-made rHDPE fiber.

Spesimen Production Process

Cantula fibers which have been soaked with 2% of NaOH for 12 hours and then dried fibers mixed with rHDPE using a mixer. Weight fraction cantula fibers comparisons were 40%, 50%, 60%, and 70%. The final mixture was put into a mold 100 mm of diameter and 10 mm thick and then pressed using 170°C of temperature for 60 minutes.

Noise Absorption Performance Testing Process

Acoustic properties testing is sound absorption performance test of material was performed by using two microphones of Impedance Tube Test in accordance with ASTM E 1050 as in Figure 1.



Gambar 1. Impedance Tube Test

Impedance tube that used was BSWA SW 422 500507 type for test specimen 100mm of diameter.

Density Testing Process

Density testing has been appropriately performed from ASTM D 792, where the testing was done by wrapping the specimens which had been cut into uniform size, using plasticine. Then, the samples were weighted in the air and fluid that has known its density.

Macroscopic Testing Process

Macroscopic testing was made by using a stereo microscope. A macroscopic is able to view the macro-structure of the specimen surface and to investigate the bond between matrix and fiber. The microscope used was Olympus Stereo Microscope SZX7 was exercised for 0.8 to 5.6 times bigger.

Data Processing Step

The first step of data processing was begun by noting the testing results into a table view on excel program. It demonstrated a graph that we were making the link between the sound absorption performance value and the frequency on various fractions. Furthermore, data obtained analysis was perfomed and supported by the density testing results and macroscopic photos.

RESULT AND DISCUSSION

Noise Absorption Performance Testing Result

The result was obtained from noise absorption performance testing at various weight fraction that can be seen on Figure 2.

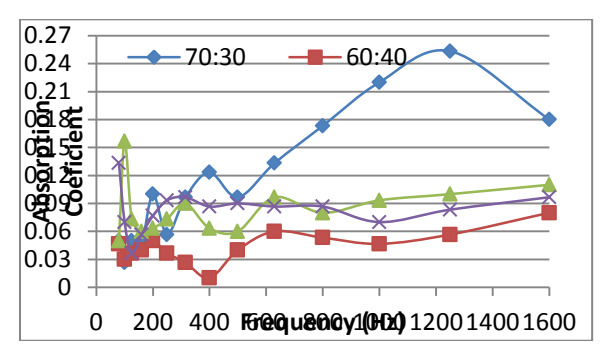


Figure 2. Noise absorption coefficient on various weight fractions

It produced 0.13 of α at 40% of composite fiber addicted on 80 Hz of frequency, whereas at 100 Hz of frequency of 50% of composite fiber addicted was 0.15 of α. At 200 Hz of frequency, 70% of composite fiber addicted was 0.1 of α. At 80-200 Hz of frequency, addicted fiber causes a frequency shift in the most optimum value of α . On 80-200 Hz of frequency data can be observed the sound absorption performance that was produced by rHDPE-Cantula composite was pretty good, it can be caused by short fibers a. As stated by Zainulabidin, et al., (2014) fiber is one kind of porous material which has a lightweight structure and fiber are cut short will have the absorption coefficient values which better than long fibers at low frequencies. The addition of fiber Cantula weight fraction did not significantly affect the value of α . However, the larger the addition of fiber optimum value α is increasingly shifted towards a greater frequency.

Greater frequency range of 500-1600 Hz graph shows the more fibers are added, the value of α will be greater. However, the composite with 60% of fibers addition are actually declined. Evenly, α is low value when compared with addition composite of 40% fiber. Basically, sound absorption phenomenon occurs when a sound wave frequency that comes together with the material natural frequency. Therefore, the sound waves energy will be absorbed and converted into heat energy through the vibrations of the material molecules (Xiaodan, et al., 2015). Each material will have a different sound absorption performance.

Density Testing Result

Density testing result is shown on Figure 3.

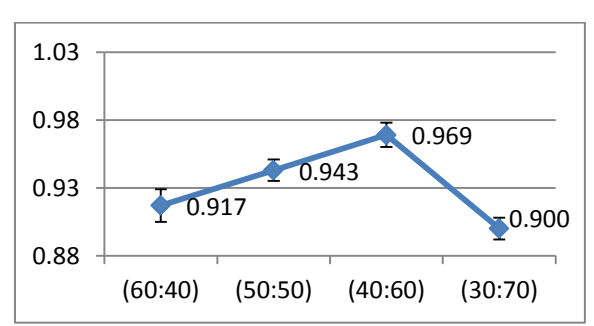


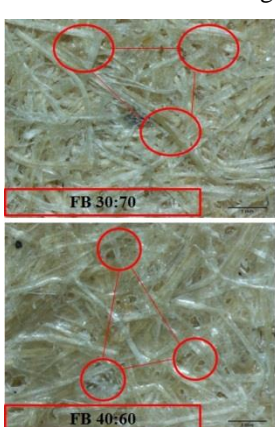
Figure 3. Density from weight fraction variation

The density testing results show fiber composites by 40%, 50%, and 60% of addition percentage increases with fiber addition. However, the density declining value in 70% fiber addition. It shows 40% and 50% of fiber addition shifts and changes a value which supported by the results of density testing that increased. Fiber addition causes greater density. It is also the friction possibility between fiber and the sound energy flow rate obstruction rose greater. Therefore, α is obtained also getting better.

Composite density in 60% of fibers addition was the greatest. It showed the best possible composition to exhibit a strong bond between fiber matrix to rHDPE cantula. The bond between the matrix and the strong fibers makes the composite becomes so dense that the material porosity is reduced which caused a material's ability to sound absorption is smaller where it is shown by the great density. Composites with 70% of fiber density addition measured value is the smallest compared to the other composites. It was possible because by the same thickness, 70% of fiber addition caused fibers presence in matrix composite become too large. Meanwhile, bond matrix less presence of fiber and matrix were caused many pores formation became weak and fragile. Therefore, it developed into the better sound absorption performance.

Macro Image Testing Result

The macro image testing was used to view the surface of each composite for each weight fraction variation as shown in Figure 4.



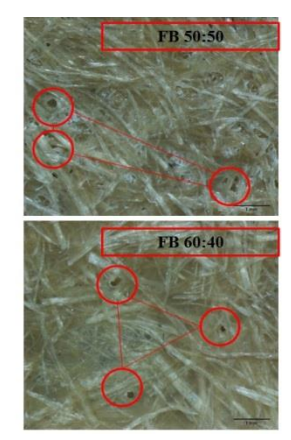


Figure 4. Macro image testing result of rHDPE:cantula composite

Composites with 70% of fibers addition by its surface was easy to investigate the cantula fiber as not coated by rHDPE matrix. It makes the composite surface which is uneven and has many gaps are formed which paved the sound waves to get into the material so that the material will be able to absorb sound better. Fiber composites with 60% of addition has a surface coated by rHDPE fiber and seen some pores on the surface so that the sound is not only absorbed on the surface but can get into the material however, solid material that causes pores was slightly formed. Therefore, the material ability to absorb sound is weak. Composite with 40% and 50% of fibers addition on the surface also seen on rHDPE coated by a matrix and contained pores so the sound waves can propagate into the material through the pores.

CONCLUSION

Based on data analysis and discussion can take several conclusions as follows:

- 1. In the 80-200 Hz frequency, the cantula fiber addition did not significantly affect to α , only caused a shift toward the optimum value of α greater frequency.
- 2. In the 500-1600 Hz frequency cantula fiber which was added then α is also getting increased. However, there were anomalies in 60% of fibers addition due to the greater density so that the material becomes more dense and the ability to absorb the sound becomes lower.

REFERENCE

- Abdullah, Y., Putra, A., Efendy, H., Farid, W. M., &Ayob, M. R. (2011). Investigation on Natural Waste Fibers from Dried Paddy Straw as a Sustainable Acoustic Absorber.In 2011 IEEE First Conference on Clean Energy and Technology CET (pp. 311-314).
- Ekici, B., Kentli, A., &Küçük, H. (2012).Improving Sound Absorption Property of Polyurethane Foams by Adding Tea-Leaf Fibers. Archives of Acoustics, 37(4), 515-520.
- Eriningsih, R. (2009). KompositSerat Rami Dan Limbah Rami SebagaiBahanAbsorpsiSuara. Arena Tekstil, 24(1), 51–59.
- Gunawan, E., Adhyaksa, A. I., &Cabuy, R. L. (2012). Influence of Sawdust Size and Ratio of HDPE Waste on The Physical Properties of Wood- Plastics Composite, Vol.: 12(04), 38-42.
- Jayamani, E., &Hamdan, S. (2013). Sound Absorption Coefficients Natural Fibre Reinforced Composites. Advanced Materials Research, Vol. 701, hal.53-58.
- Kartikaratri. Y. M., &Subagio, (2012).Pembuatankompositseratserabutkelapada n resin, 15(3), 87-90.
- R., &Yahya, I. (2014).KinerjaSerapanBunyiKompositAmpasTe bu Berdasarkan Variasi Ketebalan dan JumlahQuarter Wavelength Resonator terhadapKinerjaBunyi, 10(1), 1-5.

- F., Y., Wu, Q., Yao, &Xu, Y. (2007). Preparation and properties of recycled HDPE/natural fiber composites. Composites Part A: Applied Science and Manufacturing, 38(7), 1664-1674.
- Xiodan, Z., & Fan, X. (2015). Enhancing low frequency sound absorption of micro-perforated panel absorbers by using mechanical impedance plates. Applied Acoustics, Vol. 88, hal. 123-128.
- Zainulabidin, M. H., Rani, M, Nezere, N., & Tobi, A. (2014). Optimum Sound Absorption by Materials Fraction Combination. International Journal of Mechanical & Mechatronics Engineering, 14(02), hal.118 –121.

MANUSCRIPT WRITING GUIDELINES

Manuscript Writing Systematics

The writing sequences are as follows: title, author, and colleagues also affiliation and place of work, abstract, keyword, main article (Introduction, Research Methodology, Results, and Discussion, Conclusion), acclamation, reference, and appendix (if any). Abstracts, keywords, and content are written in English. Each abstract should not be more than 200 words. Abstract content is the subject, summary, and the conclusion of the article therefore it becomes an important document for information systems. The number of keywords is 2 to 10.

Manuscript Format

The manuscript should be typed on A-4 size of A-4 HVS paper, TNR size 10 in one column format. Margin is 2.5 cm, (top, bottom, left, and right). All pages must be numbered in sequence. The author is expected to give his writings in hard copy above the HVS A-4 as well as in the CD-R (using Ms. Word). The writing format on the CD should be the same as the hard copy. Submission of text and correspondence via electronic mail is preferred.

Equations and Units

The equations must be numbered. The serial number of the equation should be placed in parenthesis. All equations numbers must be placed on the right side of the equation and must be placed between the text. The unit used in the article is the SI unit. If other units should be used, then SI units should also be included in parenthesis. There are no special rules in the use of symbols or abbreviations, but it is recommended to use commonly used symbols. Symbols and mathematical formulas must be typed. Some symbols that provide doubt should be specified. Must be distinguished between the numbers one (1) and the letter 1 or I and between the numbers zero (0) and the letter o.

Pictures and Tables

Photos, graphs, illustrations or diagrams are included in the "Picture" group. All images and tables should be placed between the text and identified with the Latin letter (not Roman), are numbered according to the sequence (Sorting of different numbers between Figures and Tables). All letter sizes, line lengths or symbols must be uniform in black print on white and should be free of irrelevant information. All images must be clear and can be easily reduced to 50% of their original size. The typing should be clear and still read properly with 50% reduction. All tables and images must be accompanied by an explanatory legend.

Reference

The reference should be written down at the end of the article with enough information so readers can easily find it. Reference which is listed only related directly to the contents of the manuscript. Writing order: author name, year, title, publisher, and city of publication. Author name puts a family name or a reversed name, without a title. The reference literature quotes used are expressed by writing the author's name and the year published in parenthesis, for example: (Celata et al, 2000).

Associate Editor

All articles will be judged by an associate editor and will be sent back to the author along with the comments is given within one month from the date of collection. The editorial team will decide on the selection of the manuscript to be published after receiving the assessment results of the expert editing team. The editorial team is authorized to accept or reject the submitted manuscript, or to request the author to correct the manuscript. The author may provide a rebuttal to the comments/ suggestions provided by the associate editor.

Content writing is not the responsibility of the editor. All matters concerning licensing, use of computer software, script originality and other matters related to ownership and legal consequences may be the responsibility of the author. The Editor reserves the right to edit its editorial without altering the meaning and no correspondence unless the postal stamp will be returned (as it does not meet the requirements or needs to be corrected).

Each submitted manuscript shall be given a proof of loading and printing number each 3 (three) Copies. Additional requested copies or prepaid prints must be paid at special rates.